

Abstract

This work studied how in-cylinder flow structure is affected in a light-duty, swirl-supported diesel engine, when equipped with three different piston geometries: the first two featuring a conventional re-entrant bowl, either with or without valve cut-outs on the piston surface, and the third featuring a stepped-lip bowl. Particle Image Velocimetry (PIV) experiments were conducted inside an optical engine to measure swirl vortex intensity and structure during the intake and compression strokes. A full computational model of the optical diesel engine was built using the FRESKO code, a recently developed object-oriented parallel CFD platform for engine simulations. The model was first validated against the measured swirl-plane velocity fields, and the simulation convergence for multiple cycles was assessed. Flow topology was studied by addressing bulk flow and turbulence quantities, including swirl structure, squish flux, plus geometric and operating parameters, such as the presence of valve cut-outs on the piston surface, compression ratio and engine speed. The results demonstrated that conventional re-entrant bowls have stronger flow separation at intake, hampering bowl swirl, but higher global swirl than for stepped-lip bowls thanks to a stronger and more axisymmetric squish mechanism, and less tilted swirl. Stepped-lip bowls have larger inhomogeneities (tilt, axisymmetry) and higher turbulence levels, but also faster turbulence dissipation towards top dead center. They have weaker squish flux but larger squish inversion momentum as a result of the smaller inertia.

Piston geometry effects in a light-duty, swirl-supported diesel engine: flow structure characterization

Federico Perini¹, Kan Zha², Stephen Busch², Eric Kurtz³, Richard Peterson⁴, Alok Warey⁴, and Rolf D. Reitz¹

¹*University of Wisconsin–Madison, USA*

²*Sandia National Laboratories, USA*

³*Ford Motor Company, USA*

⁴*General Motors, USA*

1 Introduction

The development of fuel-efficient and environmentally friendly combustion strategies for passenger vehicle engines is being challenged by the need to meet regulatory emission mandates. Emissions are influenced by the details of the flow and combustion processes in-cylinder[1]. Most efforts have been devoted in recent years to achieve greater efficiency and lower emissions in diesel engines through complex fuel injection strategies for low-temperature combustion[2], including with multiple different-reactivity fuels[3], or near-homogeneous mixtures[4]. However, in-cylinder flow structures, which are mostly defined by the port and piston bowl design, are still typically designed for swirl-supported, conventional diesel combustion modes. Their common geometric configuration features two different-shape ports to generate a solid-body-like rotational flow (swirl) around the cylinder axis, which promotes large-scale transport of fuel vapor and air when injection occurs, as well as small-scale mixing through the generation of turbulent kinetic energy. A bowl-in-piston design aims to achieve a high bulk rotating motion to foster mixing of very rich regions of the fuel jet with the surrounding air[5].

The usage of stepped-lip piston bowls instead of omega-shaped bowls is recently becoming wide-spread in diesel engines due to superior combustion efficiency and lower pollutant emissions; however, the understanding of how flow mechanisms drive these improvements, as well as their potential for more advanced low-temperature combustion modes is not yet fully understood. Among some early studies, stepped-lip, or chamfered-lip piston geometries were found by genetic optimization[6, 7] as optimal for providing dramatically lower nitric oxides, unburned hydrocarbon as well as particulate emissions than conven-

tional bowls. It was shown that stepped-lip geometries improve air utilization especially in presence of multiple injection strategies, hence reducing emissions, as part of the fuel spray jet is directed upward in counter-rotating motion than the main in-bowl jet portion[8], or by directing the first injection towards the upper region and the second downward within the bowl[9]. Other enhancements versus conventional bowl geometries feature greater flexibility in terms of EGR usage, swirl ratio and injection spray angle[10, 11], as well as reduced convective heat transfer losses during combustion[12, 13].

This work aimed at achieving an understanding of how in-cylinder flow and turbulence structures are affected by different piston bowl designs, when no fuel injection is present. Experiments and computational modeling were performed on the Sandia National Laboratories (SNL) single cylinder light-duty diesel engine optical facility. This engine has been subject to a number of studies in recent years, aimed at characterizing low-temperature combustion strategies, analyzing the effects of different bulk swirl levels, fuel compositions, and injection timings on local mixture preparation, combustion, noise and pollutant formation[14, 15, 16, 17, 18, 19]. Three optical piston geometries were employed for characterizing flow structures during intake and compression strokes, with focus on formation of the in-cylinder swirl vortex, as well as bulk flow and turbulence availability close to top dead center. The first two geometries feature a conventional, omega-shaped, re-entrant bowl, either with or without valve cut-outs carved on the piston surface; the third features a stepped-lip bowl design.

The paper is structured as follows. First, the experimental facility, as well as details of the experimental and computational setups are summarized. Then, validation of the computational model against an in-cylinder particle image velocimetry (PIV) campaign is shown for different engine swirl ratio configurations, and at different horizontal locations within the combustion chamber during the intake and compression strokes. Next, a study of piston geometry effects was performed by first looking at qualitative intake streams and squish and swirl flow patterns; then, by analyzing quantitative flow and turbulence quantities, such as swirl ratio, turbulence availability, swirl vortex structure, squish flux. Effects of other geometric and operating parameters, such as compression ratio, engine speed, as well as presence of valve cut-outs on the piston surface were also assessed.

2 Engine setup and model details

2.1 Experimental engine setup

This study performed experiments and modeling of the Sandia National Laboratories optical light-duty diesel engine. The experimental facility features a single cylinder, optically accessible engine assembly, adapted from a production General Motors 1.9L light-duty engine, which has undergone extensive research in recent years[14, 15, 16, 17, 19]. A schematic of the experimental configuration is reported in Figure 1. The engine features optical access through fused

Table 1: Engine details.

Engine specifications	
Bore x stroke [mm]	82.0 x 90.4
Unit displacement [mm^3]	477.2
Cycle	4-stroke
Intake/Exhaust valves	2/2
Intake Valve Opening (IVO) [deg aTDC]	-359
Exhaust Valve Opening (EVO) [deg aTDC]	-152
Intake Valve Closure (IVC) [deg aTDC]	132
Exhaust Valve Closure (EVC) [deg aTDC]	360
Operating conditions	
Engine speed [rev/min]	1500
Intake pressure [bar]	1.5
Intake temperature [K]	372
Steady-state Swirl Ratio [-]	2.2, 3.5
Intake charge mole fraction [-]	10% O_2 81% N_2 9% CO_2

silica windows (50.7 mm x 25 mm), which are located at the top of the cylinder liner, as well as a fused silica piston. The only difference between the optical and corresponding production piston features is that the optical assembly has a wider crevice as well as larger top land height, which is necessary to allow imaging within the piston bowl, but slightly reduces the engine’s effective compression ratio. The cylinder liner is composed of two parts: the lower region has a drop-down design which facilitates optical alignment and cleaning when the engine is not in operation; the upper one is stationary, and is sealed against the fire-deck and the lower liner by means of O-rings on both surfaces. The in-cylinder swirl ratio can be arbitrarily adjusted by using throttle plates which are fitted in each of the intake ports, allowing to sweep effective swirl ratios from about $Rs = 1.5$ through $Rs = 5.5$, depending on the adopted throttle configuration between the helical and the tangential port, as defined by Opat[20]. Both throttle plates have the shape of their duct cross section, and are fastened on a semi-cylindrical stem. A summary of the engine’s main geometric parameters and the corresponding operating conditions used for the current study are reported in Table 1.

Piston geometries. In the study, three different piston geometries were employed, as reported in Figure 2. All meshes feature the same bowl volume of 28 cubic centimeters. The first two piston geometries, RE (or ‘re-entrant’) and RENC (or ‘re-entrant, no cut-outs’) for brevity, are derived from a 4-cylinder General Motors 1.9L light duty production engine. Both pistons feature the same omega-shaped bowl profile, which was slightly modified from the production engine in order to reduce the effective compression ratio to facilitate low

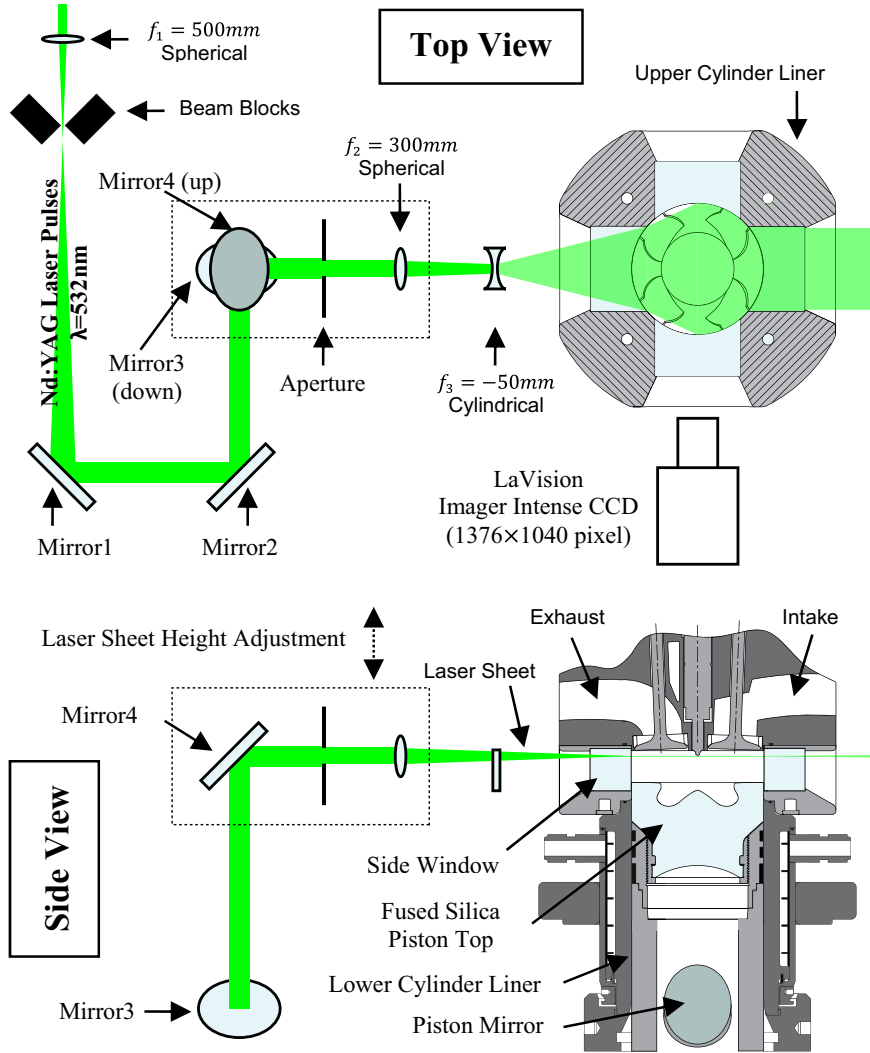


Figure 1: Schematic of the optical setup employed for swirl-plane PIV measurements. The laser sheet is shown parallel to the piston top, 3 mm below the fire-deck; piston at 50 crank angle degrees bTDC.

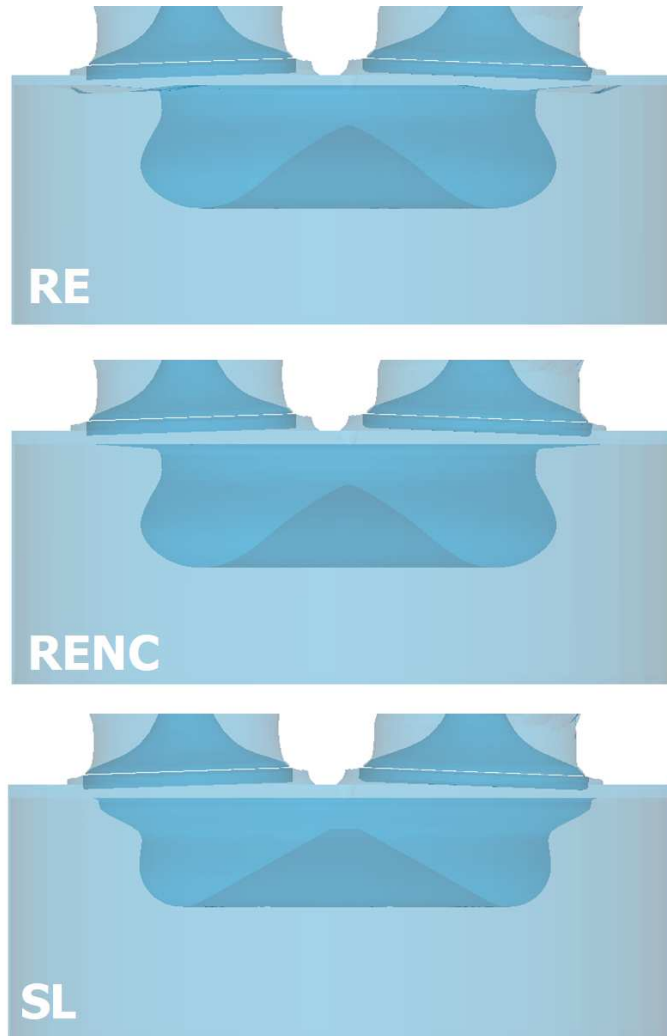


Figure 2: Piston geometries employed in the current study: from top to bottom, conventional re-entrant with valve cut-outs (RE), conventional re-entrant without cut-outs (RENC), stepped-lip (SL).

Table 2: Summary of geometric bowl properties for each piston geometry in the study: RE - re-entrant, RENC - re-entrant with no cutouts, SL - stepped-lip.

	RE	RENC	SL
Squish height [mm]	0.78*	1.36	1.36
Compression ratio	16.7	16.1	16.1
Bowl to bore ratio	0.55	0.55	0.73
Bowl volume [cm^3]	28	28	28
Valve cut-outs	Yes	No	No

* minimum

temperature combustion studies. While the original production metal piston achieves a geometric compression ratio of about 17.5, the current bowl design achieves a geometric compression ratio of about 16.7. The RE piston geometry retains the piston top valve cut-outs as well as the actual piston surface shape; the RENC configuration instead reproduces the 360-degrees sweep of the two-dimensional azimuthal average piston shape. More details on the optical piston geometry of the RE and RENC pistons are given by Colban et al.[14].

The third piston geometry features a chamfered or ‘stepped’ bowl lip (SL), as shown in Figure 2. Normal utilization of this type of bowl features splitting of the fuel spray jet into two parts, one being directed downward within the bowl, the other upward toward the head. Among the first appearances of this type of combustion geometry, genetic optimization[7] demonstrated it could reduce soot emissions and provide superior performance in presence of multiple injections; a review of its features was given by Miles and Andersson[8]. In the current study, a ‘representative’ stepped-lip bowl shape was adopted, which resembles the bowl profile design of a medium-duty piston[10], scaled to fit the 1.9L engine, so as to have the same nominal bowl volume as the corresponding re-entrant piston geometry with no valve cut-outs. The stepped-lip piston geometry has no valve cut-outs as well, both in the actual optical piston and in the computational model. A summary of the geometric details of each bowl is reported in Table 2.

2.2 Model development

In order to explore the flow structures in the engine, a high-fidelity, full engine computational model based on the recently developed FRESKO code[21] was developed.

Mesh. The combustion chamber, ports and valves, as well as the intake and exhaust runners and pressure-damping plenums, were modeled. As reported in Figure 3, an unstructured, fully hexahedral mesh was developed. The mesh retains all piston and head geometric details, including valve cut-outs on the piston surface where present, valve recesses on the head, measured injector tip protrusion into the combustion chamber, as well as the large crevice volume of

Table 3: FRESKO solver setup and numerics employed for the current study.

mesh type	body-fitted, unstructured, hexahedral
time integration	1 st -order implicit (diffusion, momentum) and explicit (advection, CFL=0.2)
diffusion accuracy	2 nd -order w/ linear interpolation
fluxing accuracy	upwind with minmod limiter
turbulence	2-eqn RNG k- ϵ
slider-crank assy.	compressible (static), $k = 0.1MN/m$

the optical assembly[14]. Wide usage was made of O-grid structures to ensure that all boundary layers in near-wall cells, especially at the liner, around the valves and valve seats, and within the ports, were not excessively skewed or tent-shaped, i.e., sharing two adjacent faces with the wall surface, as seen in the view from the top in Figure 3. Since the FRESKO solver features detailed handling of moving engine surfaces, valve interiors could be modeled using an arbitrary number of cell layers. Also, an iterative node movement algorithm ensured that aspect ratios transitioned smoothly enough through all cell layers in the combustion chamber. A total of 27 cell layers was used to discretize the valve curtain regions at maximum valve lift, in order to capture the steep velocity gradients at valve opening/closing and to ensure convergence of the flow results, as previously demonstrated[22]. That corresponds to a vertical resolution of 0.13mm. An arbitrary minimum number of squish layers was used. A value of 15 cell layers at TDC was seen to be adequate and to achieve similar or superior resolution as of a validated sector mesh model for the same engine[23]. Also, because of the compressibility of the extended optical piston assembly, a static slider-crank compressibility model with a stiffness of 0.1MN/m was employed[24].

Multiple versions of the same mesh were generated for each of the piston geometries in Figure 2 for different compression ratios, as well as for different swirl configurations of the intake throttle device, according to the previous calibration[22]. All meshes have an averaged static cell resolution of 0.7mm and feature 724055 cells at bottom dead center for the stepped-lip piston, and 682091 and 705459 cells, respectively, for the re-entrant piston with or without valve cut-outs on the piston.

Solver. The FRESKO code[21] features an object-oriented, unstructured, parallel volume-of-fluid solver for the Navier Stokes equations. The code implements closure for the turbulence terms provided by the two-equation compressible RNG k-epsilon model[25]; advanced parallel spray algorithms[26]; and the sparse analytical Jacobian chemistry solver SpeedCHEM[27, 28]. Details of the numerics employed for the simulations in this study are reported in Table 3.

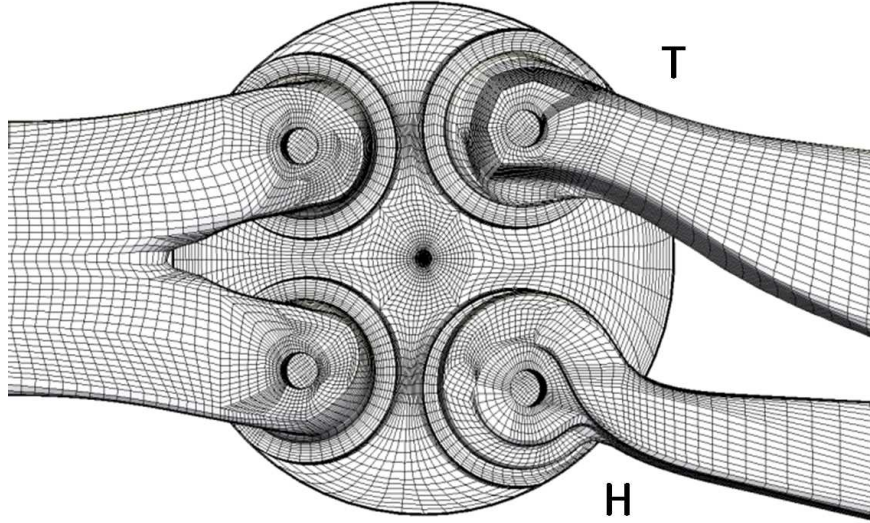


Figure 3: View of cylinder and port mesh, seen from above the cylinder head.

3 Validation

3.1 Flow topology convergence

Despite the availability of reliable boundary conditions for the simulations, a study of the flow structure evolution during multiple engine cycles was performed in order to assess how much flow initialization affects predicted flow structure, and what minimum number of simulated full engine cycles identified the best trade-off between convergence of the local flow properties during successive cycles and computational time spent for the simulations. A five-cycle simulation of the engine flows in the baseline engine configuration with a stepped-lip piston was run, from 110 to 3900 crank angle degrees aTDC. The calculation was run in parallel on 32 CPUs, and completed in 148 hours having an approximate simulation speed of about 25.5 simulated crank angle degrees per hour. This added up to slightly more than one day per simulated engine cycle. The initial crank angle was chosen during the expansion stroke and immediately earlier than exhaust valve opening (EVO). In this way, one full exhaust stroke was simulated before the first cycle started, in an attempt to minimize the effects of assuming region-averaged initial conditions by letting the strong exhaust flows properly scavenge the combustion chamber. A near-zero swirl ratio was initialized in the combustion chamber, while homogeneous and quiescent conditions were assumed in the ports, having the same thermodynamic conditions as measured at the intake and exhaust transducers.

Figure 4 shows simulated swirl vortex axis properties during multiple cycles,

according to the principal component analysis based method[29]. The swirl vortex structure appears well converged during the compression stroke for all cycles including the first one, in all three regions tested (squish, bowl, globally). However, some noticeable discrepancies appear during the intake stroke approximately between -300 and -200 degrees aTDC both in the elevation and azimuthal orientation of the swirl axis. These crank angles are critical for the swirl vortex development, as here the different patterns from the helical and tangential intake port streams merge together with complex interactions, to generate the swirl vortex – note that the global tilt angle reaches almost 30 degrees, meaning that a stable swirling vortex has not formed yet.

Even though these differences do not affect the macroscopic vortex structure later during compression, they were seen to lead to noticeable differences in local flow topology, as represented in Figures 5 and 6, confirming that a single-cycle simulation is not suitably converged for a flow study in this high-swirl engine. First, even though the average swirl axis had similar tilt, the local envelope of the swirl centers was much more wrinkled in the next cycles (for instance at 500 degrees aTDC, as from Figure 5), which also correspond to stronger intake velocities during the next consecutive cycles. On the exhaust port side – just reached by the tails of the intake port jets – stronger velocities are seen, meaning further jet penetration towards the exhaust region. The consecutive cycles do not differ much qualitatively, as just details of the jets’ outer shapes appear slightly more-or-less wrinkled.

In Figure 6, a summary of what was observed near top dead center is reported. The open-valve TDC is a crucial time frame for the prediction of trapped mass, because of the large velocities following the valve opening. Here, similar convergence behavior as in Figure 5 is seen: the first cycle exhibits weaker intake flow jets entering the combustion chamber both in the central region and at the liner sides. The second and third cycle show converged penetration of the intake jets as well as velocity magnitude patterns. Closed-valve TDC showed even better convergence, with virtually no differences among all cycles.

These findings suggest that a satisfactory trade-off between computational demands and the need for accurate flow predictions can be reached by simulating two full cycles, the first having been initialized by a full exhaust stroke simulation. The creation of a stable, strongly swirling vortex seems to justify such efficient convergence of the flow simulations. However, the validity of the current findings may not be general to other engine configurations characterized by significantly different flow structures, where more complex flow interactions could take place.

3.2 In-cylinder velocity fields

The accuracy of the converged flow predictions was tested by comparing to the in-cylinder PIV measurements of Zha et al.[19, 30]. The experimental measurements were taken at multiple intake port configurations, which yielded bench-equivalent swirl ratios of $Rs=2.2$ and $Rs=3.5$; the baseline, non-throttled engine configuration corresponding to a bench swirl ratio $Rs=2.2$. PIV measurements

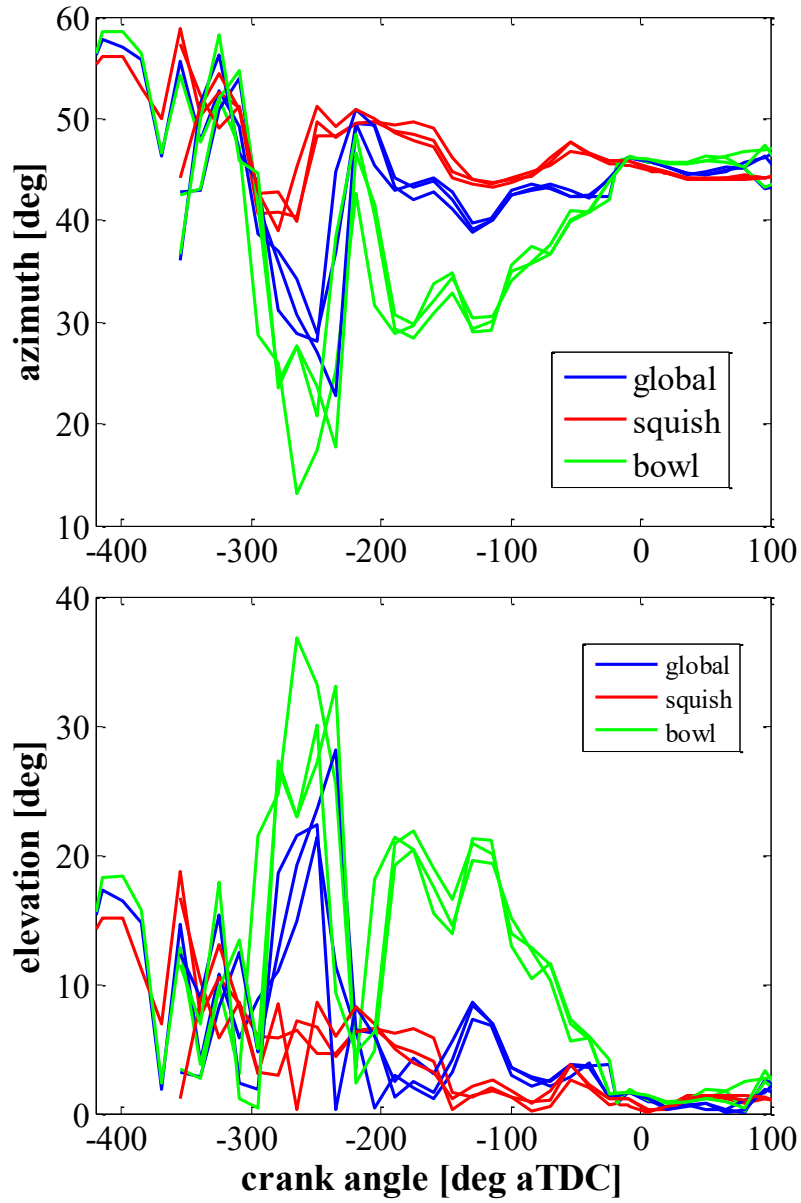


Figure 4: Swirl vortex principal components during the first three simulated cycles: (top) swirl axis azimuthal orientation, (bottom) swirl axis tilt angle with the cylinder axis.

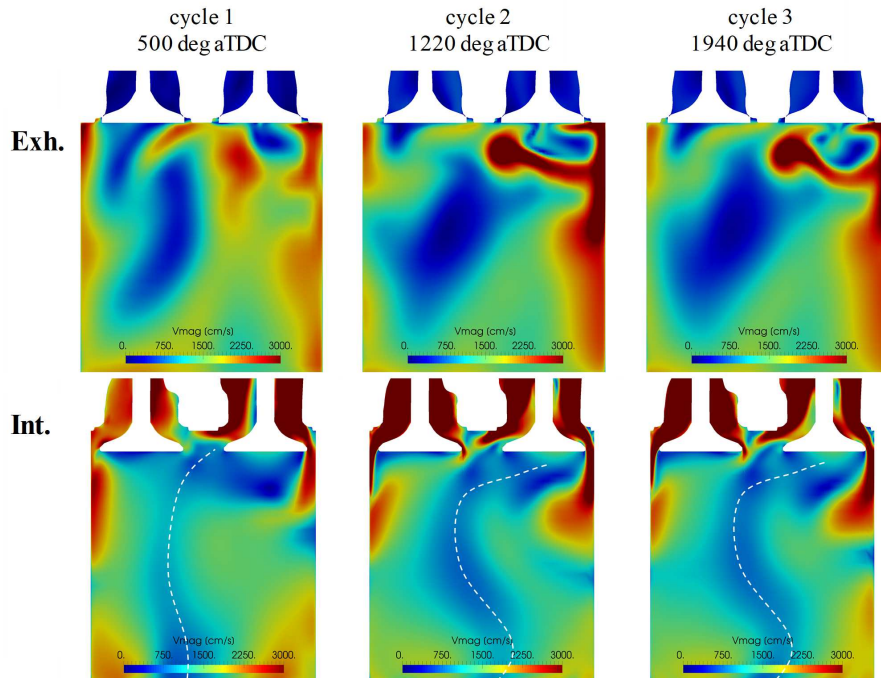


Figure 5: Flow simulation convergence during the intake stroke at -220 deg aTDC: vertical cross section below the exhaust (top) and intake (bottom) valves, respectively.

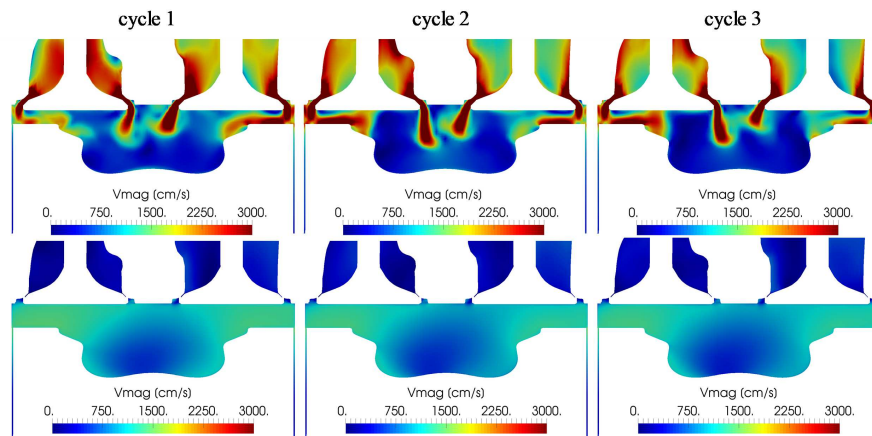


Figure 6: Flow simulation convergence near top dead center: vertical cross section below the intake valves, early intake stroke at -340 deg aTDC (top) and during closed-valve part at -25 deg aTDC (bottom), respectively.

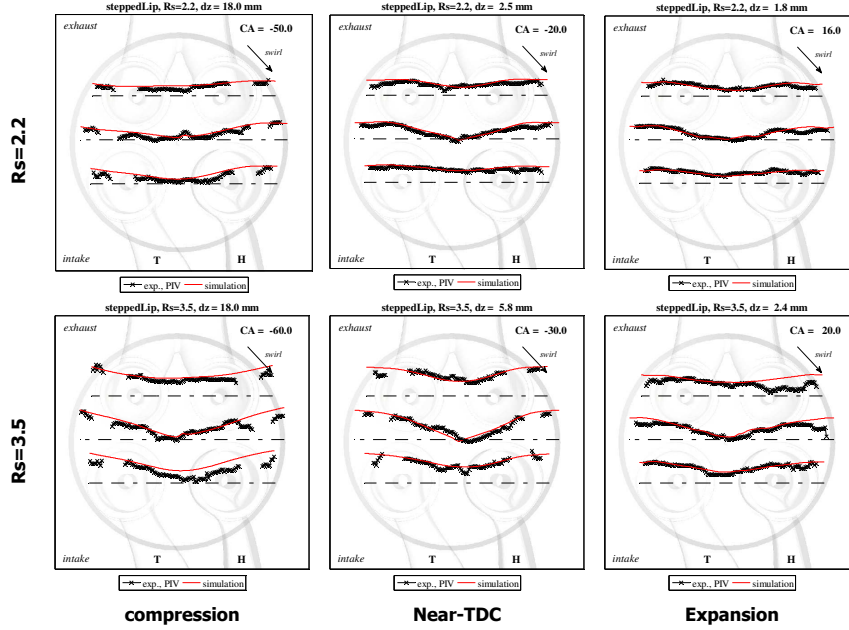


Figure 7: Predicted versus measured tangential velocity profiles at three line-of-sight locations in a horizontal plane halfway within the squish, during compression and early expansion. Stepped-lip piston, $Rs=2.2$ (top) and 3.5 (bottom).

in the experimental facility were taken at every fifteen crank angle degrees during both the intake and the compression strokes, at different horizontal plane locations within the combustion chamber, according to a newly developed optical distortion correction methodology[31].

Figures 7 and 8 report a selection of tangential velocity profile comparisons between ensemble-averaged PIV and the simulations for the stepped-lip and reentrant piston geometries, respectively. The observations were made towards the end of the compression stroke up to until the very early exhaust stroke, at a horizontal plane location located between 18mm and 1.8mm from the fire-deck, during each case approximately halfway within the squish region. The plots represent quantitative comparisons of tangential velocity components at three lines of sight on the same horizontal plane: one located along the line which connects the intake valve stems, one symmetrically splitting the cylinder, the last one running below the exhaust valves. The tangential – swirling – velocity component s is computed based on the two-dimensional cartesian velocity

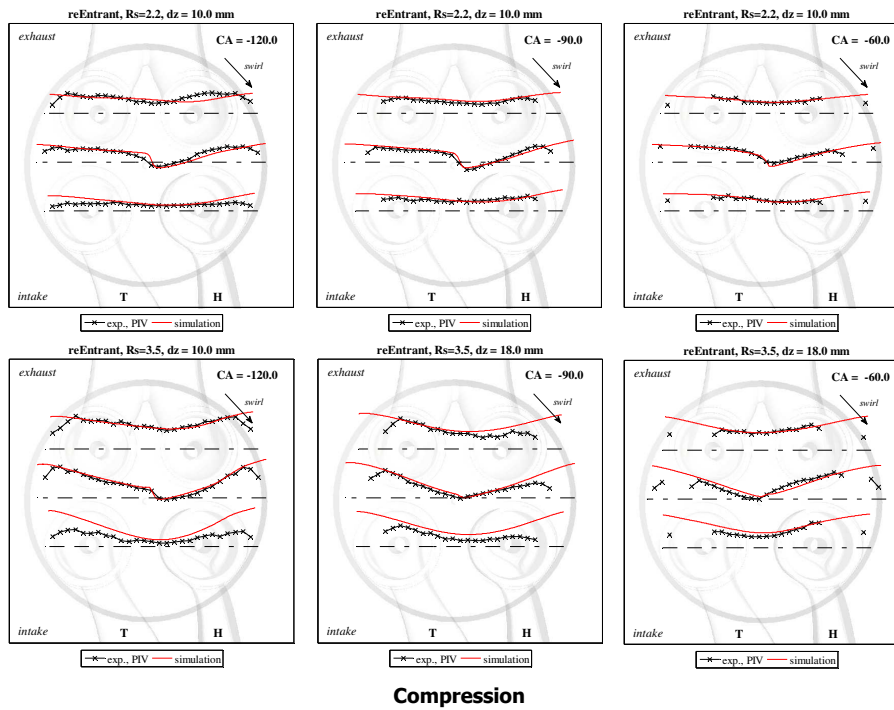


Figure 8: Predicted versus measured tangential velocity profiles at three line-of-sight locations in a horizontal plane halfway within the squish, during compression and early expansion. Conventional Re-entrant piston, $R_s=2.2$ (top) and 3.5 (bottom).

components (u, v) and cylindrical coordinates (θ, r) as

$$\begin{bmatrix} -r \sin \theta & \cos \theta \\ r \cos \theta & \sin \theta \end{bmatrix} \begin{bmatrix} \dot{\theta} \\ \dot{r} \end{bmatrix} = \begin{bmatrix} u \\ v \end{bmatrix} \quad (1)$$

$$s = \dot{\theta}r. \quad (2)$$

Both piston geometries exhibited acceptable accuracy of the simulations at the two swirl ratio tested, $Rs=2.2$ and $Rs=3.5$. One outer annular region of the stepped-lip combustion chamber in Figure 7 had zero measured tangential velocities because of the severe distortion caused by the bowl step; however, overall, tangential velocity profiles were well captured across all lines of sight, including the swirl center locations in the central line, which can be identified approximately by where the tangential velocity is zero. For both swirl ratios, the peak tangential velocities close to the cylinder walls were correctly captured. Similar behavior was seen for the re-entrant piston in Figure 8, even if some slight deviations were seen for the highest swirl ratio of $Rs=3.5$ and early compression stroke case, at -120 deg aTDC crank angle. At this crank angle, shortly after intake valve closure the simulation slightly over-predicted tangential velocities below the tangential intake port. Also, the measurements showed some unphysical decrease in magnitude close to the walls, which was identified by Zha et al.[31] as the effect from severe laser background reflection from the cylinder liner at crank angles far enough from top dead center.

The PIV measurements provided useful data also to assess the in-cylinder precessive motion of the swirl vortex, as reported in Figure 9. Here, predicted and measured swirl center locations at various horizontal planes above the piston top located 10 mm far from the fire-deck during the late compression stroke are reported. These planes are located in the upper region of the combustion chamber at the crank angles analyzed; hence, the swirl center at this location represents motion of the upper tip of the in-cylinder swirl vortex axis. The simulation correctly captured motion from the helical port side towards the tangential port side, as well as from the intake port side towards the exhaust port side when the piston is approaching TDC. The precessive movement is more evident with the stepped-lip geometry, where larger motion along the x-axis was seen towards the exhaust port. Also, for the stepped-lip geometry, the swirl center speed is non uniform, with slower motion occurring from -60 to -45 degrees aTDC, where the swirl center only moves by a few millimeters; and faster motion later, as the piston moves closer to top dead center. With the re-entrant piston, similar motion along the y-axis is seen, i.e., the swirl center moves from the tangential towards the helical port area, close to the geometric center. However, the swirl center moves almost along a straight line. Overall, the simulations are seen to provide acceptable accuracy for assessing the flow structure at any in-cylinder location. Some discrepancies are seen for the late crank angles with the re-entrant piston, where the simulation predicts some wrinkling of the swirl center path. In a recent study [32], simulations with additional two-equation turbulence models highlighted that renormalized k-epsilon models cannot capture wrinkles in the inner swirl core well, despite the

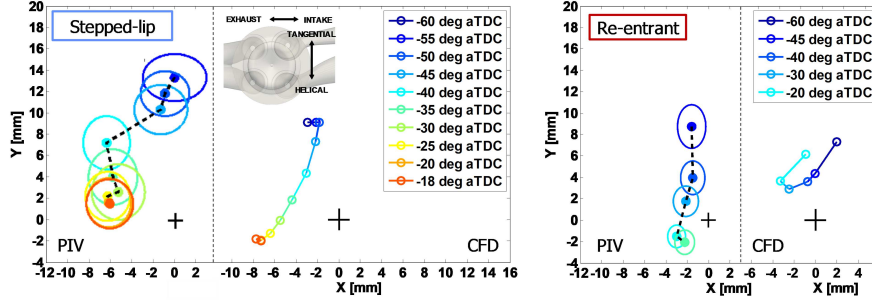


Figure 9: Swirl center locations at a horizontal plane 10mm far from the fire-deck: PIV ensemble-averaged data with one standard deviation circles versus 2nd-cycle FRESKO predictions, (left) stepped-lip and (right) re-entrant piston geometry. 2d plane X axis: positive side towards intake, negative towards exhaust port. Y axis: positive side towards tangential intake port, negative towards helical port. Origin: cylinder axis.

computational mesh being highly resolved close to the swirl axis. The standard k-epsilon model yielded significantly better agreement, but proved unsuitable for diesel engine simulations involving sprays and combustion.

4 Results

4.1 Flow structure

The swirl vortex shape and the squish momentum transfer mechanism are important measures to evaluate the in-cylinder flow structure during the late compression stroke. Hence, a suitable velocity field decomposition was adopted:

$$\mathbf{u} = \mathbf{u}_{swirl} + \mathbf{u}_{squish}, \quad (3)$$

and evaluated on a vertical cross-sectional plane which splits the combustion chamber between the two intake ports. The tangential, or swirling, velocity components are given by the normals to the cross-sectional plane, which has normal vector \hat{j} :

$$\mathbf{u}_{swirl} = (\mathbf{u} \cdot \hat{j}) \hat{j}; \quad (4)$$

while the squish velocity vectors are the remaining velocity components, lying on the plane surface:

$$\mathbf{u}_{squish} = \mathbf{u} - \mathbf{u}_{swirl} = \mathbf{u} - (\mathbf{u} \cdot \hat{j}) \hat{j}. \quad (5)$$

Figures 10,11,12 report the corresponding flow decomposition at three relevant crank angles during the final half of the compression stroke, through TDC, where fuel injection and mixture formation would occur for most injection strategies,

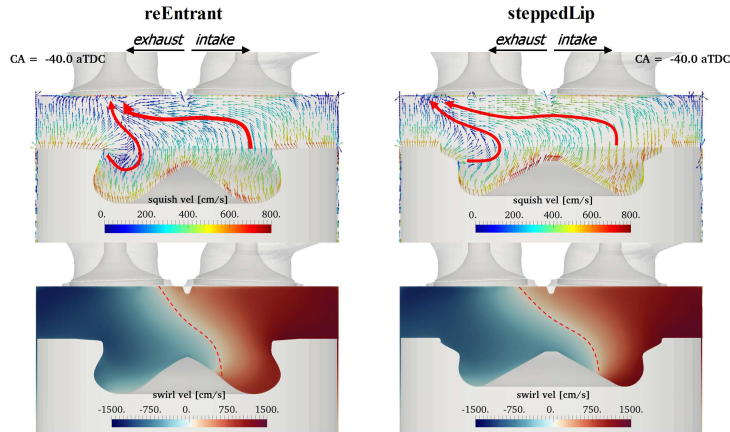


Figure 10: Flow structure during compression stroke at -40 deg aTDC on a vertical cross-sectional plane with a (left) re-entrant or (right) stepped-lip piston. Top row: squish velocity; Bottom row: tangential velocity component.

and where the effects of piston geometry on flow structures are stronger because most of the combustion chamber volume is represented by the piston bowl at these times. At 40 crank angle degrees before TDC, as in Figure 10, piston geometry is not affecting the flow structure significantly yet. Both piston geometries exhibit the same squish velocity pattern, with streams departing from the surroundings of the bowl rim upwards towards the exhaust valve region; and no signs of an axisymmetric squish flow pattern are evident yet, even though some velocity components at the bowl rim are already pointing downward in the re-entrant bowl. Also, both swirl vortex axes show similar tilting angles towards the exhaust side, even though to a slightly larger extent for the stepped-lip bowl vortex. In Figure 11, at 20 degrees bTDC, differences between the two piston configurations become more evident. The conventional re-entrant bowl has already created a stable squish flow structure, where charge from the outer squish region is being pushed inward towards the bowl as an azimuthally symmetric tumbling vortex centered at the bowl rim. Instead, the stepped-lip bowl engine still retains the non-symmetric flow structure generated by the intake stroke: a first squish vortex stub is forming at the inner bowl step rim below the exhaust valves, but stable radial streamlines directed upward and towards the exhaust valve region are still present in the whole azimuthal sector below the intake valves. The much larger flow non-uniformity appears affected by two major causes: by first, the weaker squish flow strength, mostly due to the larger rim radius, as more thoroughly discussed later. Second, the stepped-lip shape is divergent along the inward radial direction, causing flow expansion along the squish streamlines, which reduces the flow velocities and the efficiency of the squish mechanism. The larger flow non-uniformity with the stepped-lip piston is conserved through top dead center, as reported in Figure 12. A weak tum-

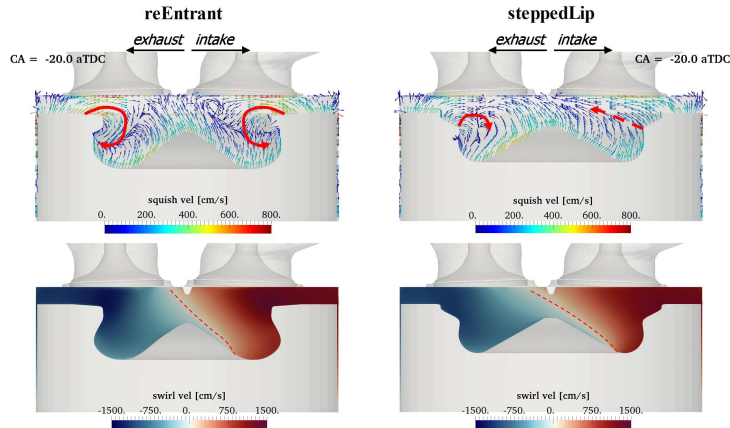


Figure 11: Flow structure at 20 deg bTDC on a vertical cross-sectional plane with a (left) re-entrant or (right) stepped-lip piston. Top row: squish velocity; Bottom row: tangential velocity component.

bling vortex is eventually occupying the inner bowl region below the exhaust valves. The vortex is not fully enclosed in the inner bowl well, but more broadly reaches also the step region. Again, the whole azimuthal sector below the intake valves is not covered by a coherent squish vortex yet, as the vortex center stub is still dominated by the shear layer between two radial streams: a top one directed towards the squish, and a bottom one traveling along the inner bowl surface, towards the center of the cylinder. Instead, the conventional re-entrant piston exhibits a strong, azimuthally symmetric, tumbling vortex within the omega-shaped deeper regions of the bowl.

Piston geometry effects on flow structure were observed also early during the intake stroke, despite the piston surface being far and moving farther from the head, as reported in Figure 13. As highlighted in a previous study[22], the intake flow from the tangential port creates a large, bore-scale vortex through a stream which enters the cylinder straight from the port, i.e., along a tangential direction, and pointing slightly downward. As the piston movement fosters more air to enter the cylinder, the tangential port stream eventually impacts against the piston surface, and is driven towards the bowl. The conventional re-entrant and the stepped-lip geometries exhibit noticeably different behavior at this time. With a conventional bowl, the large horizontal annular region of the piston top surface causes the flow to deviate to an almost horizontal orientation, then causing a sharp flow separation as the stream enters the bowl. This flow structure closely resembles that of the academic ‘backward facing step’, or ‘sudden flow expansion’ flow configurations. An independent recirculation bubble is fully formed within the bowl, where the impact happens. With a stepped-lip bowl instead, the piston squish area is much smaller, and the tangential port stream is less severely tilted. Furthermore, the presence of a step towards the

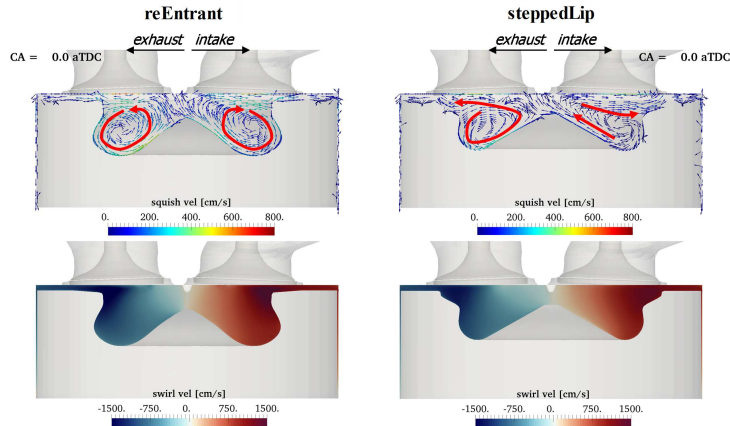


Figure 12: Flow structure at top dead center on a vertical cross-sectional plane with a (left) re-entrant or (right) stepped-lip piston. Top row: squish velocity; Bottom row: tangential velocity component.

bowl makes the path towards the bowl well much smoother. Hence, very limited – if at all – flow separation occurs here, and much larger swirling velocities enter the bowl region at this stage.

This observation has two implications. First, a ‘scavenging’ process takes place, as – during fired operation – combustion products still located within the bowl after the end of the intake stroke will account for most of the internal residuals, as already observed in Perini et al. [22], where a non-homogeneous temperature stratification of about 15 K was seen to survive at TDC with a conventional re-entrant bowl as a result of incomplete scavenging. In this sense, the stepped-lip piston appears more capable of scavenging the bowl region from the combustion products from a previous cycle. Second, different swirl ratio behaviors build up within the bowl. As also represented in Figure 14, the presence of the recirculation bubble in the conventional piston geometry hampers swirl formation within the bowl, which causes greater separation in swirl behavior between the bowl and the squish throughout the whole intake and compression strokes. With a stepped-lip bowl, much greater and faster swirl ratio development in the bowl is seen. However, due to its more open shape, pressure wave effects in the stepped-lip combustion chamber also lead to greater swirl ratio oscillations, apparently as a result of momentum transfer between the bowl and the squish regions. Also, the swirl ratio effect in the bowl is second-order in comparison to the impact squish flow has on near-TDC swirl amplification. Despite a lower bowl swirl, the conventional re-entrant piston has a globally higher near-TDC swirl ratio of about 10% more than for the stepped-lip piston.

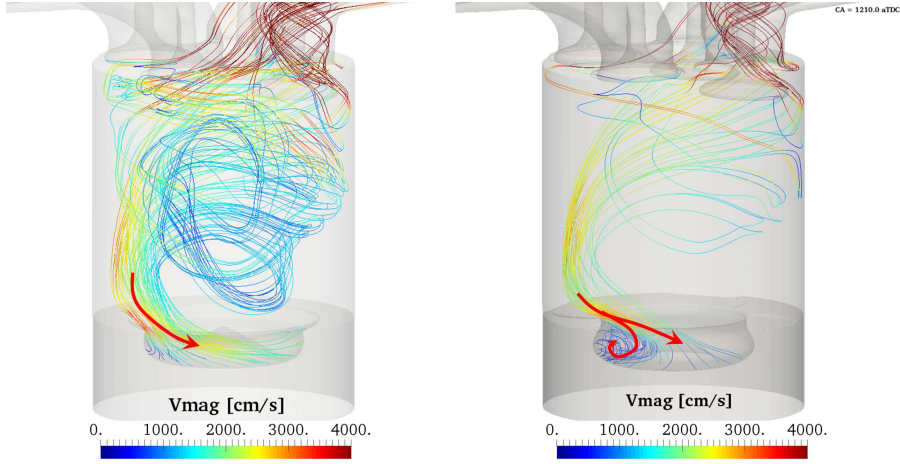


Figure 13: Visualization of different flow separation behavior via streamlines at -230 deg aTDC: (left) stepped-lip bowl, (right) conventional re-entrant bowl. Red arrows highlight flow patterns in the bowl impact region. Streamlines computed via backward integration, after initialization within the piston bowl.

4.2 Bulk flow quantities

In order to quantify the effects of the different flow patterns observed, region-based averaging of flow quantities of interest to combustion design was performed, according to the approach developed in Perini et al.[29]. Time-resolved region-average values are obtained either by volume or by mass averaging of the local field quantities enclosed in the bowl volume, in the squish volume, or globally within the combustion chamber. ‘Near-TDC’ quantities were also defined in order to provide approximate values which would characterize the charge when injection would occur. These values are defined as the time averages over the crank angle range between -50 deg aTDC and +10 deg aTDC.

Swirl ratio. Bulk region-based swirl ratios were computed as:

$$Rs|_{\Omega} = \frac{\sum_{i \in \Omega} [m_i (x_i - x_c) v_i - m_i (y_i - y_c) u_i]}{\omega \sum_{i \in \Omega} [m_i (x_i - x_c)^2 + m_i (y_i - y_c)^2]}, \quad (6)$$

where ω represents the crank’s rotational speed, m_i and $\mathbf{x}_i = (x_i, y_i, z_i)$ the mass and node position associated to each momentum cell i in the domain Ω , and $\mathbf{x}_c = (x_c, y_c, z_c)$ the coordinates of the center of mass for the whole set:

$$\mathbf{x}_c|_{\Omega} = \frac{\sum_{i \in \Omega} m_i \mathbf{x}_i}{\sum_{i \in \Omega} m_i}. \quad (7)$$

The time-resolved swirl ratio comparison between a conventional re-entrant bowl with cut-outs and the stepped-lip bowl are reported in Figure 14. Here, the two piston geometries exhibit extremely similar swirl ratio trends globally, as well as for the squish region, throughout the whole intake stroke and most of the compression stroke. The late compression stroke through TDC exhibits instead different swirl amplification mechanisms, as highlighted in Figure 15: beginning approximately 90 degrees before top dead center, the conventional bowl allowed greater swirl build-up, leading to a higher swirl ratio in the squish region and globally. This finding is in line with the angular momentum conservation principle, which relates greater swirl amplification for the conventional bowl geometry with lower bowl-to-bore ratio and thus smaller moment of inertia.

Swirl ratio in the bowl instead exhibits a different behavior. Swirl development in the conventional bowl is much slower during the intake, and it is associated to intake flow separation at the piston surface and the formation of a recirculation bubble which inhibits the formation of a swirling vortex. With a more open stepped-lip bowl, no separation occurs, and the swirl ratio builds up faster within the bowl; it also exhibits a secondary oscillatory behavior, apparently responding to momentum transfer due to pressure wave effects between the bowl and the squish region. However, the conventional re-entrant bowl achieves superior swirl ratio at top dead center because of a more efficient squish flux mechanism, as will be explained in the next section.

Turbulence. In-cylinder turbulence kinetic energy somewhat mirrors the swirl ratio behavior, as reported in Figure 16. The stepped-lip geometry achieves higher turbulence energy than the the conventional re-entrant one in all regions. As from the qualitative flow structure analysis, the stepped-lip geometry features larger flow inhomogeneities within the combustion chamber all the way through to top dead center. This is linked to greater conversion into turbulent structures and steadily higher turbulence levels. However, this phenomenon also leads to faster turbulence dissipation, which becomes evident close to top dead center. Here, the turbulence intensity peak happens earlier for the stepped-lip geometry, and the steeper turbulence dissipation leads to lower turbulence levels thereafter. However, the piston-induced cold flow turbulence benefit achieved throughout the cycle and faster dissipation should not be overemphasized, since fuel injection during fired engine operation may lead to higher turbulence levels.

Compression ratio/squish height effects. Figures 17 and 18 report the near-TDC quantities for varying geometric compression ratios. In this analysis, TDC squish heights were varied from an allowable minimum, which avoided interference with the valves, up to larger values which achieved similar compression ratios across the different piston geometries. For both piston geometries with no valve cut-outs, the maximum feasible compression ratio was of 16.1, corresponding to a TDC squish height of 1.36 mm, while the conventional bowl with valve cut-outs could be exercised also at its nominal compression ratio of

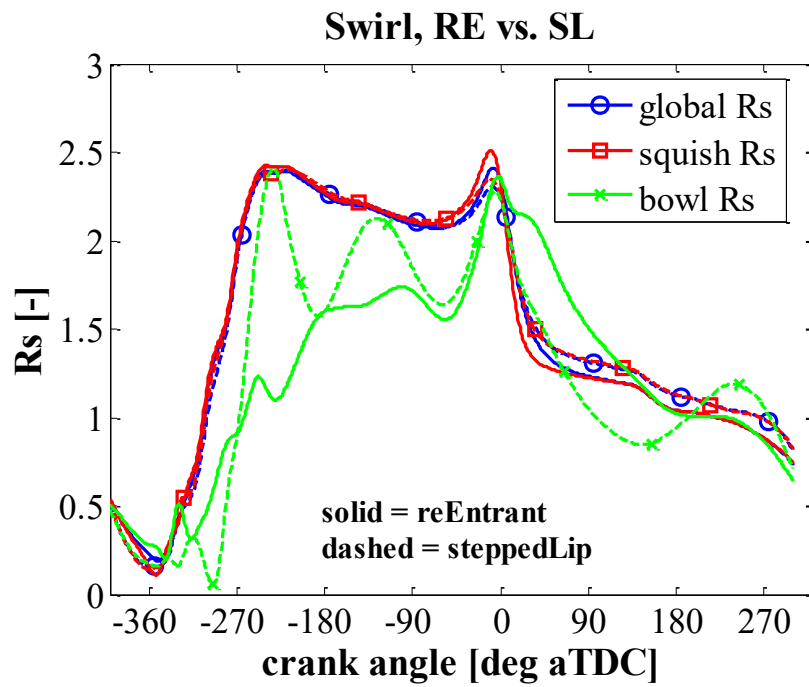


Figure 14: Region-averaged (squish, bowl, global) swirl ratios versus crank angle for conventional re-entrant (solid lines) and stepped-lip (dashed lines plus marks) geometries.

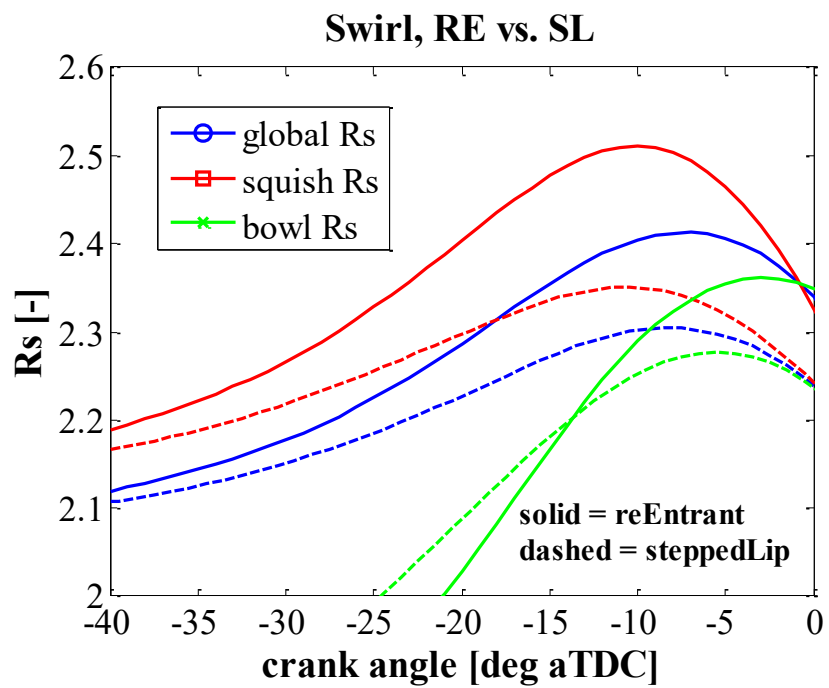


Figure 15: Predicted near-TDC swirl ratio growth for for conventional re-entrant (solid lines) and stepped-lip (dashed lines) geometries.

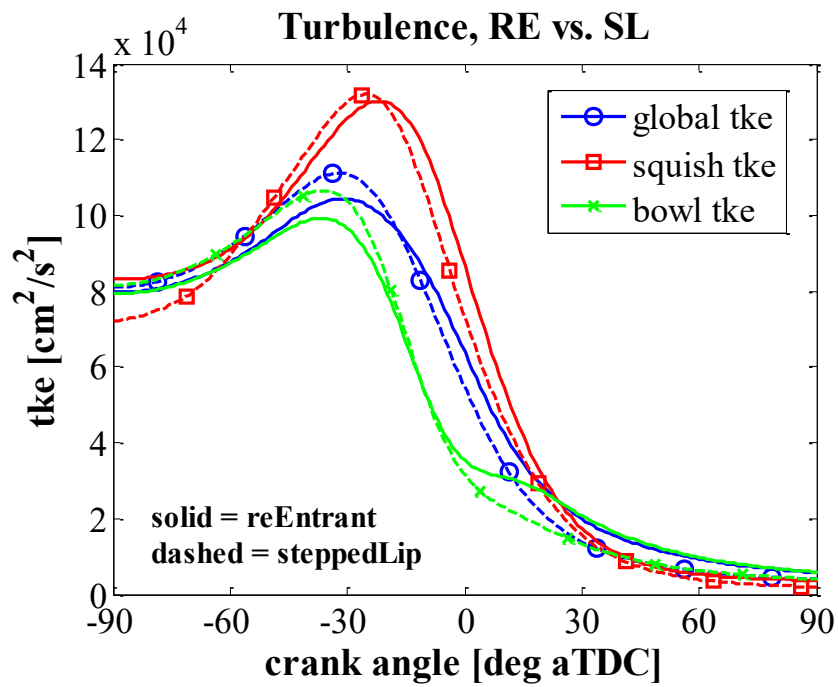


Figure 16: Region-averaged (squish, bowl, global) turbulence kinetic energy versus crank angle for conventional re-entrant (solid lines) and stepped-lip (dashed lines plus marks) geometries.

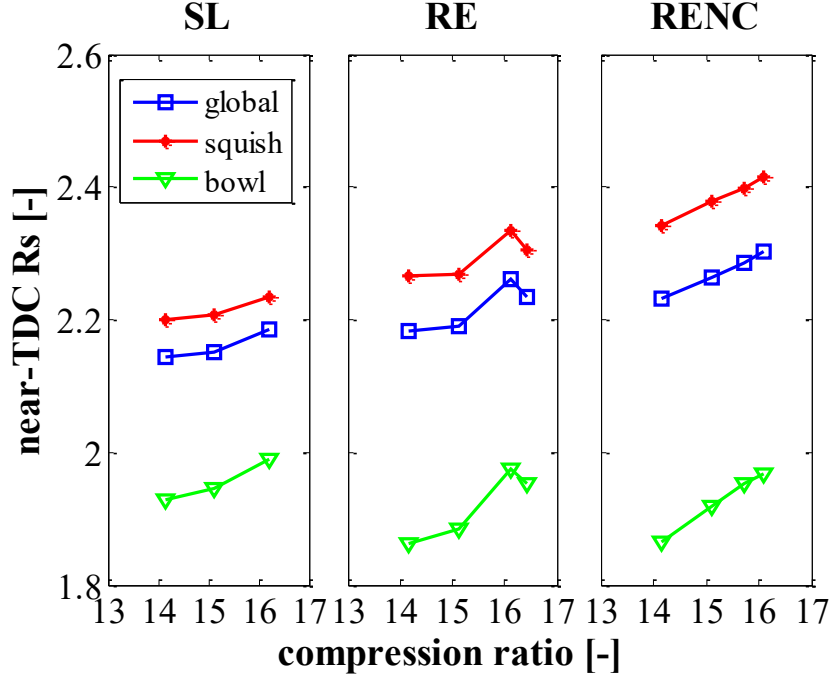


Figure 17: Compression ratio effect on bulk near-TDC average swirl ratio.

16.7, having a minimum squish height of 0.78 mm. Since this geometry has a non-even piston surface, this latter value is not averaged, but represents a minimum value measured from the top of the piston surface and the cylinder head. Both plots highlight a reasonably smooth and nearly linear correlation of the near-TDC quantities with compression ratio. In all geometries, increasing compression ratio essentially leads to a more active bowl flow due to a stronger squish flux mechanism: both swirl ratio and turbulence kinetic energy increase significantly in the bowl, which drives their increase globally. For the re-entrant piston geometry with no cut-outs, it was interesting to observe that the version with valve cut-outs exhibits an opposite trend when moving from 16.1 to the nominal 16.7: the better thermodynamic properties achievable with the highest compression ratio come at some price in terms of flow quantities for mixing, as a result of the much smaller squish volume left and greater proximity of the solid wall boundaries on the flow near top dead center.

4.3 Squish flux structure

In order to quantify how much the different squish mechanisms arising from each piston geometry affected the overall flow structure and turbulence avail-

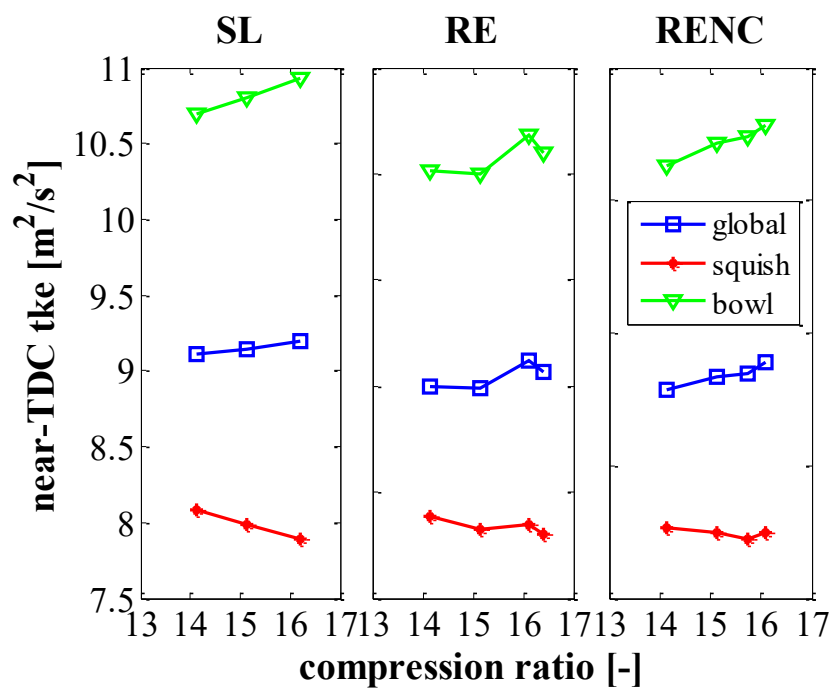


Figure 18: Compression ratio effect on bulk near-TDC average turbulence kinetic energy.

ability towards the end of the compression stroke, a methodology based on three-dimensional simulation data was developed. A squish flux curtain surface is defined as the envelope of all cell faces, obtained looping through all the piston bowl rim edges, all the way up to the cylinder head, as reported in Figure 19 where the contour plot on the curtain surface represents the local squish mass flux. Quantities at each face centroid of this cylindrical surface, such as area normal, density and velocity vector are available from the CFD solution. These local data highlight that, even in presence of a globally positive (i.e., from the outer squish region towards the bowl) or negative (from the bowl towards the outer radial direction) squish flux, local oscillations and also changes in sign happen because of the initial flow non-uniformity introduced through the helical and tangential port flow patterns.

A global squish flux formulation is given by the flux integral over the curtain surface:

$$\phi_S = \int_S \rho \mathbf{u} \cdot \hat{n} dS \approx \sum_{i=1}^{n_f} \rho_i (\mathbf{u}_i \cdot \mathbf{A}_i); \quad (8)$$

similarly, an average squish velocity u_{sq} can be obtained:

$$u_{sq} = \frac{\phi_S}{\int_S \rho dS} \approx \frac{\phi_S}{\sum_{i=1}^{n_f} \rho_i A_i}. \quad (9)$$

The line integral of the two-dimensional curtain flux data along the cylinder axis direction provides an average azimuthal squish flux formulation, which characterizes the squish flow structure when the piston is reasonably close to top dead center, and the squish height is small. Piston geometry comparisons at 50 degrees bTDC and at top dead center are reported in Figures 20 and 21, respectively. In Figure 20, at 50 crank angle degrees bTDC, the piston still owns a non-negligible velocity, but the squish height is still large, which highlights the effects of non-uniformities. Here, all three piston geometries are still affected by the intake flow structure, i.e., larger squish velocities are seen entering the center of the cylinder from the upper-right corner, where the helical intake port is located. However, much larger azimuthal in-homogeneity is seen for the stepped-lip piston, where squish velocities reach zero on the diametrically opposite side, below the exhaust valves, in the azimuthal regions where the valve seats carved on the piston head surface determine an expansion basin that reduces the effects of the squish flow. Both conventional re-entrant pistons exhibit stronger and more uniform squish flow instead, and the version with no cutouts has slightly stronger squish below the intake valves because of the locally smaller squish height. At top dead center, both geometries share the same squish pattern. However, the stepped-lip geometry not only shows smaller squish velocity magnitudes, but it also exhibits eight distinct low-squish peaks in the locations where the squish flux curtain intersects the valve seats. The valve recesses on the cylinder head were confirmed to be responsible for this phenomenon by looking at various plots for crank angles near TDC, which highlighted that the azimuthal locations of these peaks are nearly constant between the end of the compression stroke and the early expansion.

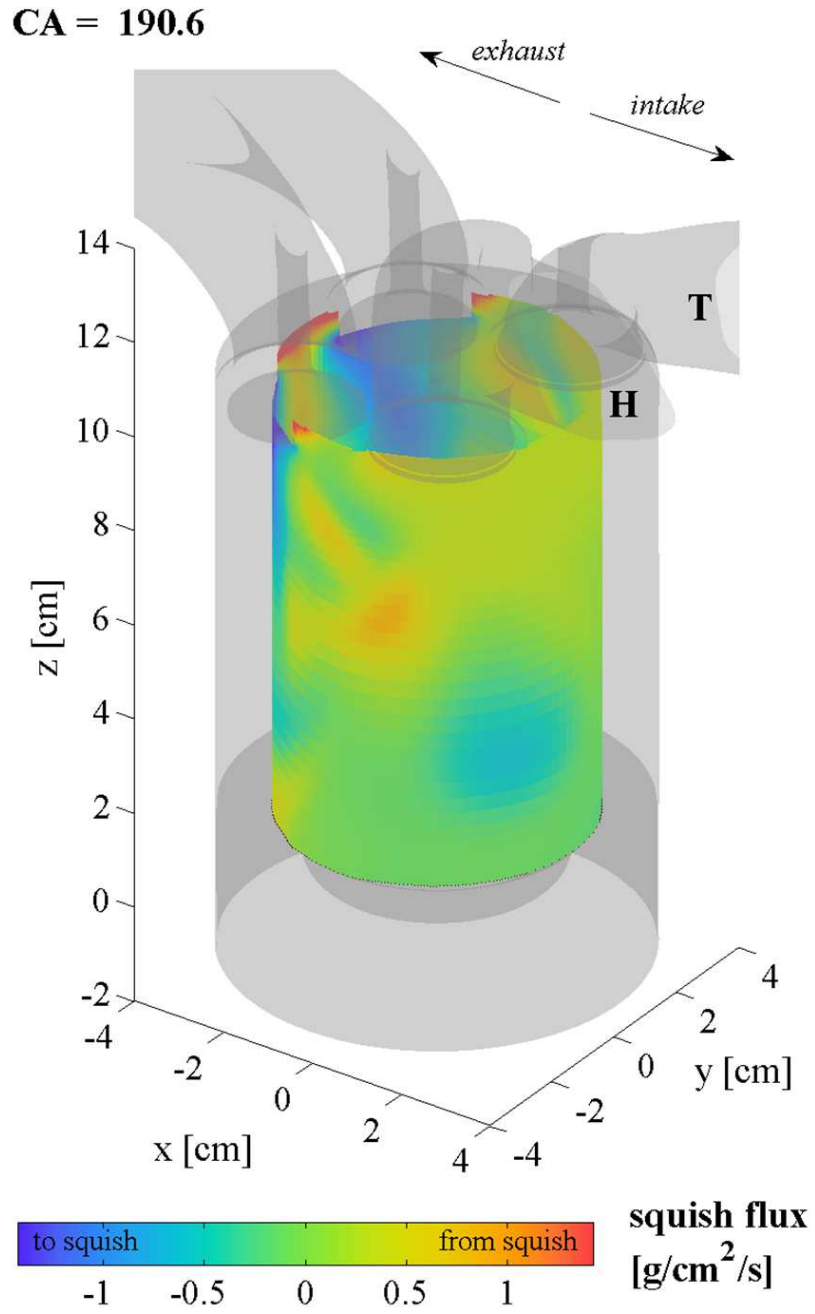


Figure 19: Squish flux curtain definition imaging. SL bowl geometry during the exhaust stroke.

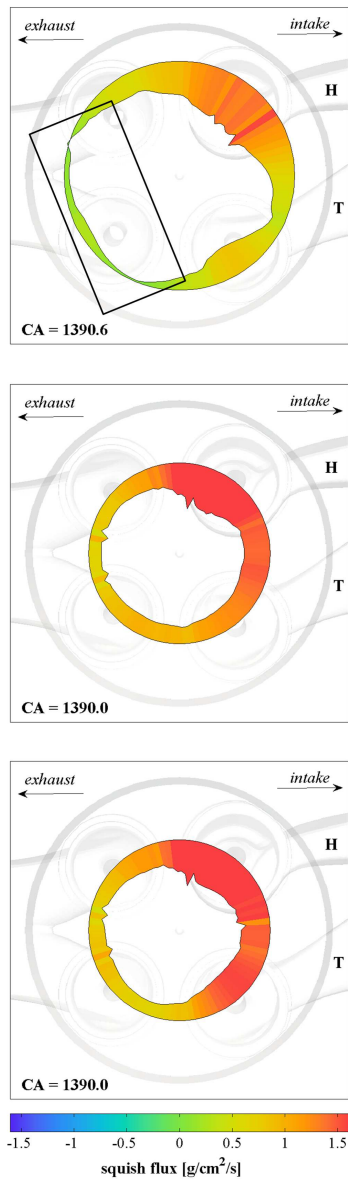


Figure 20: Squish flux patterns during compression at 50 deg bTDC. Piston geometries: (top) stepped-lip, (center) re-entrant, (bottom) re-entrant with no cut-outs. .

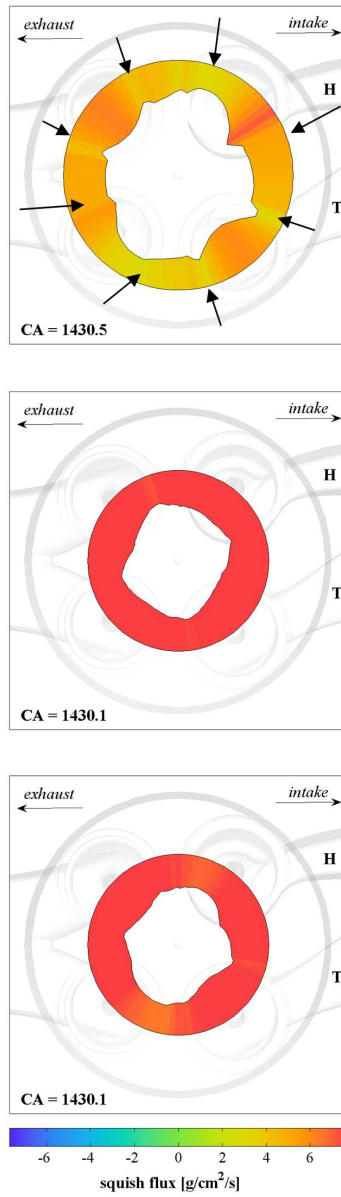


Figure 21: Squish flux patterns near top dead center. Piston geometries: (top) stepped-lip, (center) re-entrant, (bottom) re-entrant with no cut-outs. Arrows highlight lows of squish flux corresponding to sudden flow expansions at the valve seats.

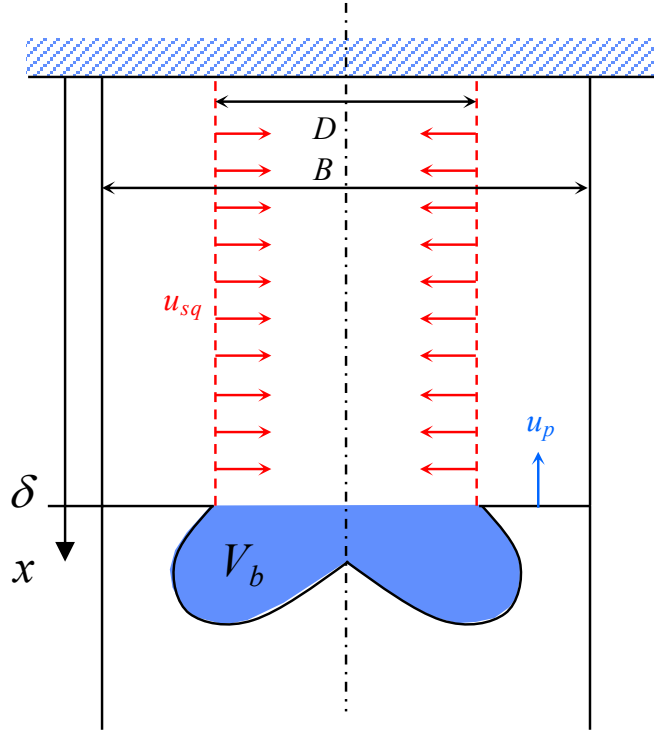


Figure 22: Schematic of one-dimensional squish flux model.

In order to relate the instantaneous squish velocity obtained through Equation 9 to a maximum squish velocity which could occur at the same conditions in the engine, an ideal squish flux model was developed by extending the model of Heywood[33] to piston bowls of generic shape. A schematic of the squish mechanism assumed by the model is reported in Figure 22.

The instantaneous squish velocity u_{sq} is assumed uniform over the curtain surface, and the fluid density is assumed uniform throughout the whole combustion chamber. B and D define the piston bore and the bowl rim diameter, respectively, u_p and δ the instantaneous piston velocity and piston surface distance from the fire-deck, V_b the bowl volume, independent of bowl shape. The simplified combustion chamber geometry assumes a flat outer piston surface and flat head. In order to compute an instantaneous squish velocity, the model solves the one-dimensional mass conservation equation surrounding the inner control volume, '1', given by the region enclosed by the squish curtain surface towards the interior:

$$\frac{\partial M_1}{\partial t} = 0 = \frac{\partial}{\partial t} \int_{V_1} \rho dV + \int_S \rho \mathbf{u} \cdot \hat{\mathbf{n}} dS. \quad (10)$$

According to this equation, the ratio of the instantaneous squish velocity to the instantaneous piston speed is given as

$$\frac{u_{sq}}{u_p} = \frac{B^2 - D^2}{D\delta \left(4 + \frac{\pi B^2 \delta}{V_b}\right)}; \quad (11)$$

and is function only of the geometric parameters of the combustion chamber and of the piston bowl. In particular, with the same cylinder bore B , $u_{sq}/u_p \propto V_b (1 - D/B)^2$, hence the squish mechanism can be enhanced by either reducing the bowl rim diameter to a smaller fraction of the bore, or by increasing the piston bowl volume. In the current study both piston bowl geometries have the same volume; then, expected squish performance could be based only on the different bowl rim radii:

$$\frac{u_{sq,RE}}{u_{sq,SL}} \approx 2, \quad \frac{\dot{M}_{1,RE}}{\dot{M}_{1,SL}} \approx 1.5. \quad (12)$$

The multidimensional simulation results are reported in Figure 23. The one-dimensional model of Equation 11 provides a maximum squish flux that the engine could exploit to stabilize the near-TDC flow structure. Hence, a squish ‘efficiency’ coefficient was defined as the ratio between predicted (3d) and modeled (1d) squish intensity, in order to measure how far the squish mechanism with the actual bowl was differing from the ideal case, and to give an idea of how inefficient the squish mechanism was because of the non-homogeneity of the intake flow structure and geometric details of the piston bowl:

$$\varepsilon = u_{sq}/u_{sq,1D}. \quad (13)$$

According to the results of Figure 23, the pistons exhibit two distinct behaviors when being close or far enough (approximately 20 degrees) from TDC. Far from TDC and throughout most of the compression and expansion strokes, the stepped-lip piston geometry has a noticeably smaller squish efficiency than the conventional re-entrant pistons, which perform in a similar way in both the with- and without-cutouts configurations. The inefficiency gets worse farther from top dead center. This confirms that the larger rim radius and the more open bowl shape are less prone to constraining the swirl vortex into a well-centered, azimuthally symmetric configuration, which would more effectively suppress the azimuthally non-homogeneous velocity components descending from the intake stroke. Very close to TDC, squish ‘inversion’ takes place, as the radial flow switches from inward to outward following the change in sign of piston speed. Here, the squish efficiency is higher for a stepped-lip piston, because of the smaller inertia that has to be overcome when the squish flux switches from positive to negative as the piston velocity changes sign. This mechanism appears fostered by the greater flow non-homogeneity, which was already shown to lead to higher turbulence levels in-cylinder. This could favor mixing, or at least an easier scavenging of the squish region immediately after top dead center, ideally close to start of the high temperature heat release.

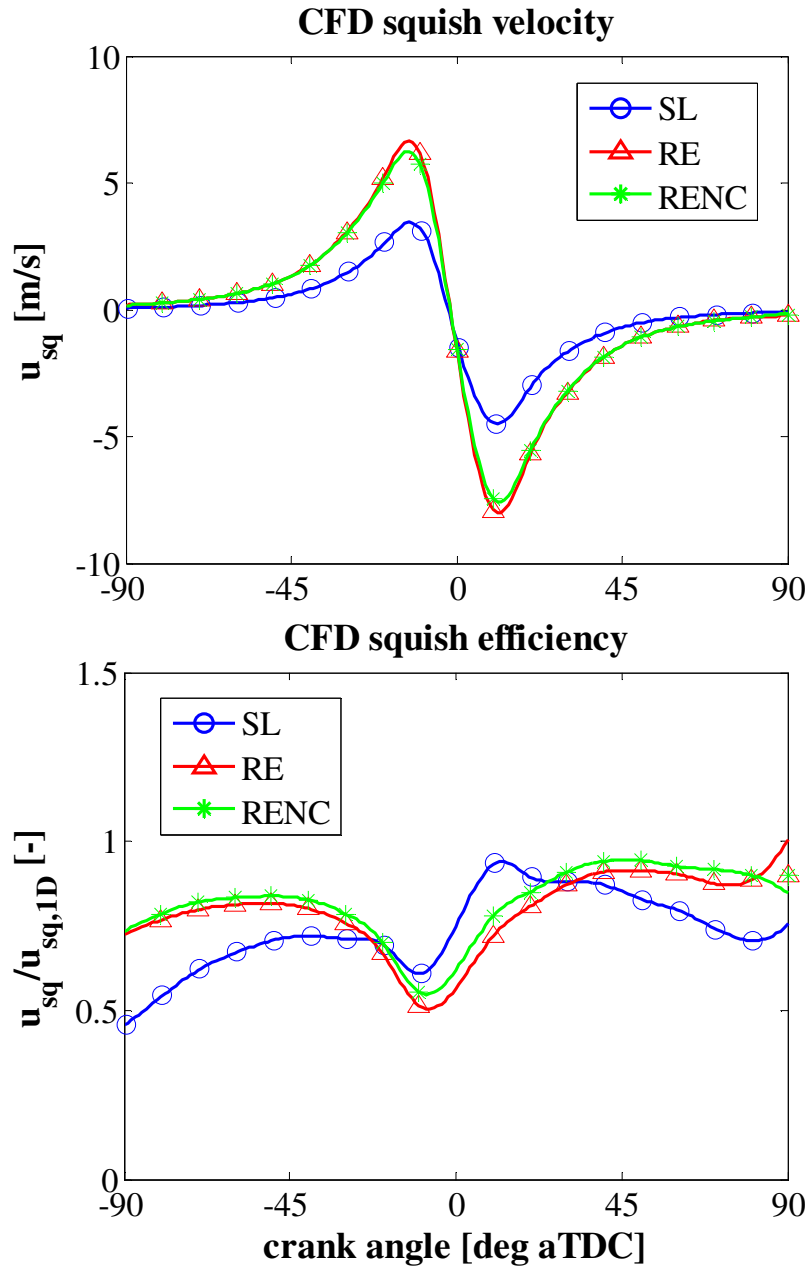


Figure 23: Squish performance near TDC for all piston geometries: (top) 3D squish velocity, (bottom) squish efficiency.

Table 4: Summary of fitting coefficients for region-averaged near-TDC swirl ratio and turbulence kinetic energy according to Equation 14.

		RE	RENC	SL	SL vs. RE
α	global	0.35	0.31	0.34	
	squish	0.38	0.32	0.36	
	bowl	0.30	0.26	0.29	
β	global	1.35	1.55	1.46	
	squish	1.35	1.59	1.51	
	bowl	1.31	1.40	1.28	
γ	global	0.578	0.565	0.599	+3.6%
	squish	0.473	0.466	0.493	+4.2%
	bowl	0.396	0.398	0.419	+5.8%

4.4 Effect of engine speed

The engine’s rotational speed was swept from $n = 700rev/min$ up to $n = 3000rev/min$ in order to assess flow structure dependency on the average piston speed, $\bar{u}_p = 2\pi n/60$. All calculations showed similar flow structures at the relevant crank angles previously studied. All flow fields exhibited similar flow patterns, but have different velocity magnitudes depending on each case’s engine speed, suggesting that engine speed in the typical operating range of a light-duty diesel does not affect the overall flow structures noticeably. To verify this hypothesis, the two relevant quantities of near-TDC region-averaged swirl ratio and turbulence kinetic energy were assessed versus the average piston speed value, as reported in Figures 24 and 25, respectively. Both quantities exhibited smooth behavior versus engine speed, hence suitable fitting formulas could be drawn:

$$\begin{aligned}
 Rs_{TDC} &= \alpha\sqrt{\bar{u}_p} + \beta, \\
 K_{TDC} &= \gamma\bar{u}_p^2.
 \end{aligned}
 \tag{14}$$

The results are summarized in Table 4: all swirl ratios scale with the square root of the average piston speed, while all TDC turbulence kinetic energies correlate well with the average piston kinetic energy. Both re-entrant bowl geometries achieve higher TDC swirl ratios than the stepped-lip at all speeds; near-TDC turbulence kinetic energies are instead higher for the stepped-lip geometry, even if the improvement is never larger than about 6%.

4.5 Effect of valve cut-outs

Finally, the effect of the presence of valve cut-outs on the piston surface was studied. Valve cut-outs are a necessary geometric detail to maximize the engine’s compression ratio, while avoiding physical interference between the valves and the piston surface during the valve overlap period. However, their presence

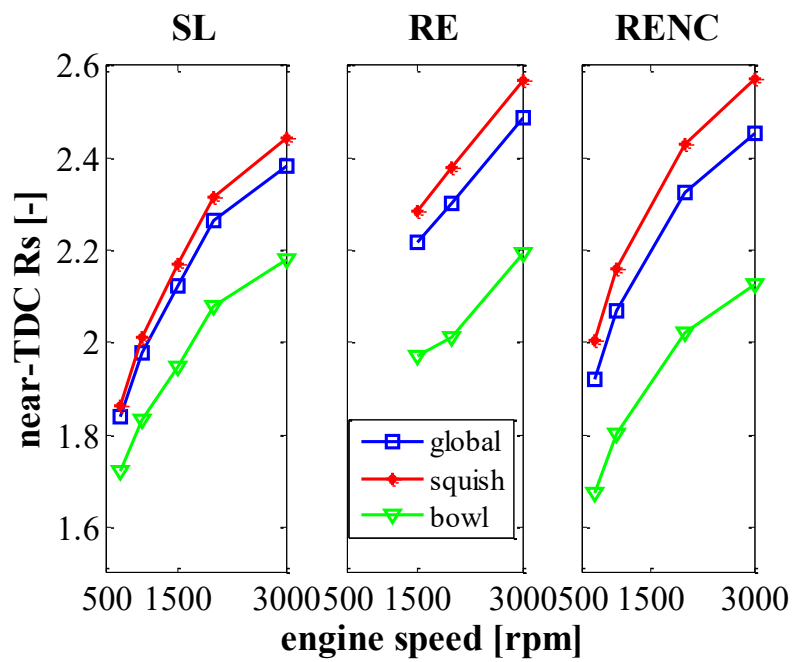


Figure 24: Effects of engine speed on near-TDC swirl ratio, from 700 to 3000 rpm.

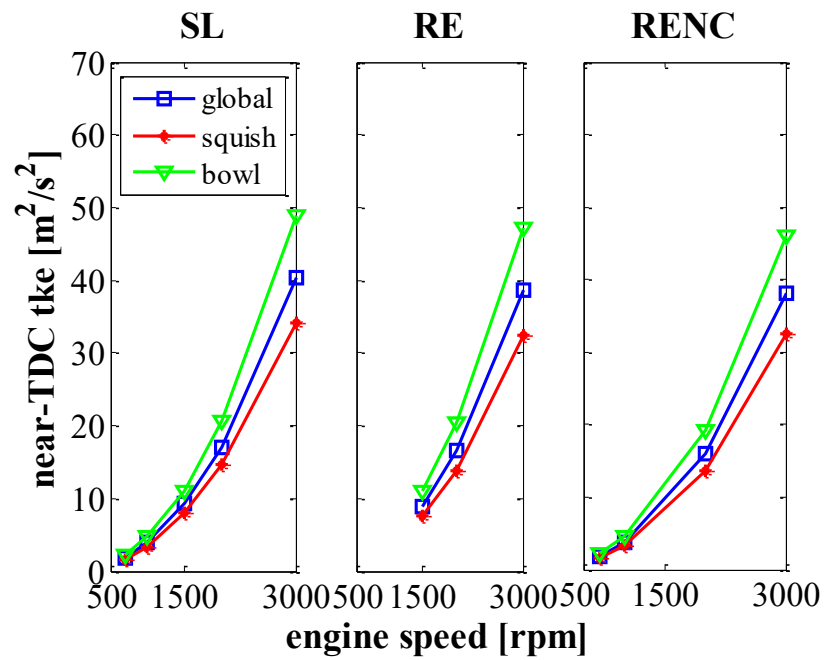


Figure 25: Effects of engine speed on near-TDC turbulence kinetic energy, from 700 to 3000 rpm.

makes the path for early intake flow streams more complex, with potential for larger volumetric efficiency losses. The details of a conventional re-entrant piston when either equipped with valve cut-outs or not, are reported in Figure 26.

Comparisons between the two piston geometries were done for the same engine compression ratio, $CR=16.1$. This compression ratio was chosen as it is the geometrically feasible maximum for the piston having no cut-outs in order to avoid interference with the valve movement. As already shown in Figures 17 and 18, the presence of valve cut-outs introduces some non-linear behavior at higher compression ratios, where TDC squish heights in the piston surface sectors between the valves are locally of the order of 0.5 mm, which suggests for strong interaction of the piston and head wall boundary layers.

Most of the effects of valve cut-outs on the flow structure were observed to happen during the early phases of the intake stroke, during valve overlap, when the piston is extremely close to top dead center, as reported in Figure 27 for the bulk swirl ratio. Here, the piston with cut-outs reaches a lower swirl ratio minimum, apparently because of the more complex path the intake streams experience entering the cylinder: the piston surface is not flat, but regains its height a few millimeters outside of the valves. Hence, the intake stream experiences a stronger deviation. Furthermore, squish height is smaller outside of the valves than in the flat piston surface with no cut-outs, reducing the engine's breathing at this stage. These deviations also lead to some flow differences in the bowl region, where the piston without valve cut-outs exhibits a slightly earlier and more coherent development of a tumbling vortex due to the intake flow, which could negatively compensate for the amount of swirl profit earned in the squish region, as represented in Figure 28.

The swirl ratio profit earned by the piston with no valve cut-outs during the early intake stroke was seen to hold, almost unvaried, all the way to the next top dead center – close to which there is a slight amplification phenomenon. TDC swirl ratio in the squish region was 2.650 and 2.541 for the version without and with valve cut-outs, respectively. Globally, i.e., including also the almost unaffected bowl region, a smaller difference of 2.465 versus 2.434 was seen.

5 Concluding Remarks

The in-cylinder flow structure has been characterized in a light-duty, swirl-supported diesel engine, when equipped with pistons featuring either a conventional re-entrant bowl, or a stepped-lip bowl. A computational model of the Sandia National Laboratories single-cylinder optical facility was built using the FRESKO code. The model was validated against PIV measurements of in-cylinder local velocity fields during the intake and compression strokes, with both piston geometries, and at different horizontal locations within the combustion chamber. Then, simulations were performed to assess the effects of the two piston geometries on the flow structure, with focus on near-TDC quantities of interest for mixing and combustion development, when fuel injection is present.

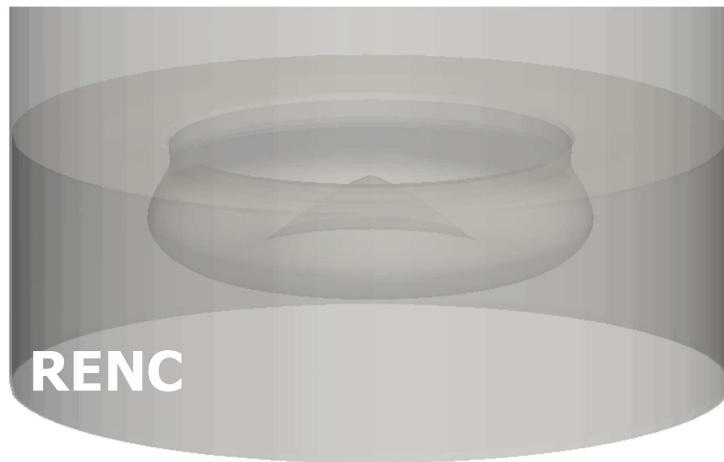
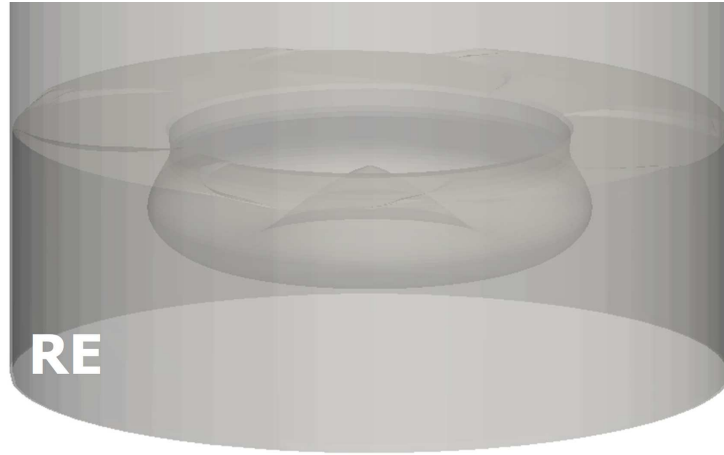


Figure 26: Details of the conventional re-entrant pistons with (top) or without (bottom) valve cut-outs.

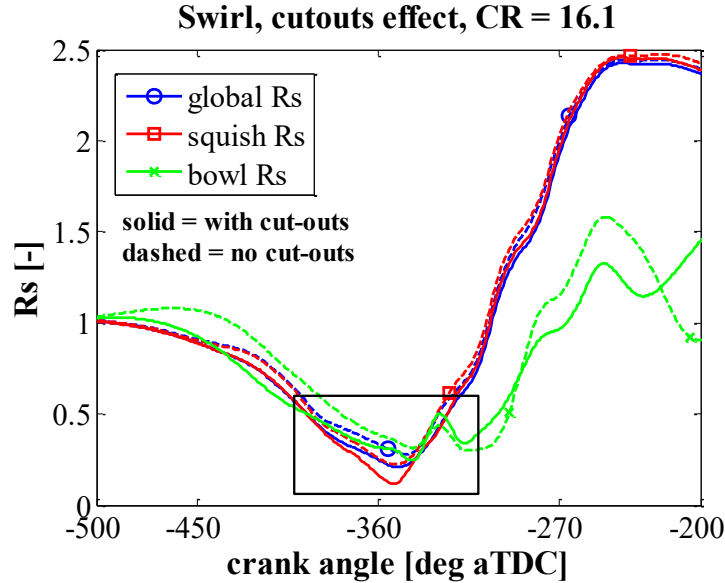


Figure 27: Effect of valve cut-outs on intake stroke swirl ratio, early intake part highlighted with a black box.

Based on the study, the following conclusions could be drawn:

- conventional re-entrant piston bowls have more severe flow separation from the tangential port stream, which hampers swirl formation in the bowl, and could lead to larger internal residuals during fired operation. However, their more enclosed shape leads to a stronger squish flow, which leads to a globally stronger near-TDC in-cylinder swirl, approximately 10% larger than for stepped-lip bowls;
- stepped-lip bowls have a more open shape which allows for larger swirl axis tilt and lesser flow axisymmetry, as long as more of the flow non-uniformities descending from the dual intake port geometry are retained until top dead center. This leads to higher turbulence levels than for a conventional bowl during the intake and compression strokes, but also faster turbulence dissipation. Hence, lower turbulence kinetic energy is seen at TDC than for a conventional bowl;
- squish flow is considerably stronger for the conventional bowl geometry; a stepped-lip bowl has a less homogeneous squish flux pattern, which reduces its inertia when the piston velocity changes sign. This results in greater squish ‘efficiency’ near TDC, whose implications on injection and combustion behavior have yet to be verified;

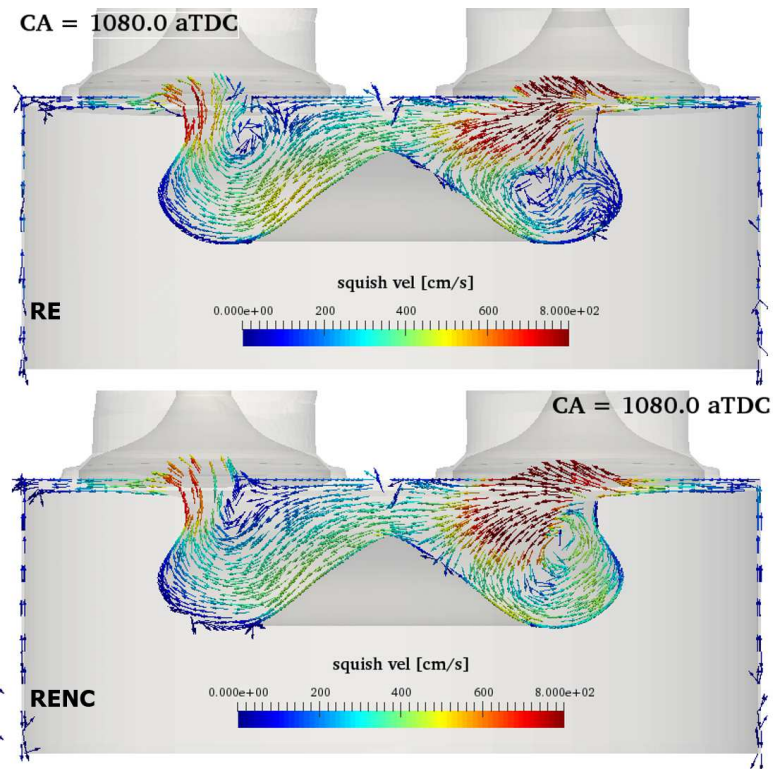


Figure 28: Effect of valve cut-outs on squish flow structure at top dead center during the early intake stroke: pistons (top) with valve cut-outs, (bottom) without valve cut-outs.

- valve cut-outs on the piston surface generate a more complex stream path early during the intake stroke, when large velocities enter the cylinder through the intake valves and impact against the piston surface. This accounts for a slight reduction (-1.3%) in swirl ratio and an increase in higher turbulence kinetic energy ($+4.6\%$) at TDC. Different swirl ratio development during the intake is evened out by the late-compression squish flow;
- engine speed and compression ratio do not affect the flow structures, as bulk flow and turbulence quantities scale smoothly with these parameters.

The study also highlights recommendations for the multidimensional simulation of swirl-sustained diesel engine flows:

- in the presence of strong swirl vortices, RANS simulations of engine flows can be considered 'converged', i.e., providing an optimal trade-off between computational demand and accuracy of the predicted flow structures, starting from the second full cycle after having been initialized at exhaust valve opening;
- experimentally-derived tangential velocity profiles are very closely reproduced by the simulations where the PIV data are expected to be reliable, i.e., reasonably far from wall regions where severe background scattering occurs and the annular regions where complex optical paths crossing the bowl lip deteriorate measurements.

On-going efforts are focusing on understanding how each piston geometry affects mixture formation, combustion development and pollutant formation via enhanced flow patterns, scavenging, and air utilization, when fuel injection is present.

acknowledgments

The authors wish to acknowledge support for this research provided through the Sandia National Laboratories by the U.S. Department of Energy, Office of Vehicle Technologies, program managers Leo Breton, Gupreet Singh. Sandia National Laboratories is a multi-program laboratory managed and operated by Sandia Corporation, a wholly owned subsidiary of Lockheed Martin Corporation, for the U.S. Department of Energy's National Nuclear Security Administration under contract DE-AC04-94AL85000. ANSYS Inc. is also gratefully acknowledged for providing licenses of the ICEM-CFD mesh generator.

References

- [1] Reitz RD. Directions in internal combustion engine research. *Combustion and Flame* 2013; 160(1): 1 – 8. DOI:<http://dx.doi.org/>

- 10.1016/j.combustflame.2012.11.002. URL <http://www.sciencedirect.com/science/article/pii/S001021801200315X>.
- [2] Musculus MP, Miles PC and Pickett LM. Conceptual models for partially premixed low-temperature diesel combustion. *Progress in Energy and Combustion Science* 2013; 39(2-3): 246 – 283. DOI:<http://dx.doi.org/10.1016/j.pecs.2012.09.001>. URL <http://www.sciencedirect.com/science/article/pii/S0360128512000548>.
- [3] Reitz RD and Duraisamy G. Review of high efficiency and clean reactivity controlled compression ignition (rcci) combustion in internal combustion engines. *Progress in Energy and Combustion Science* 2015; 46: 12 – 71. DOI:<http://dx.doi.org/10.1016/j.pecs.2014.05.003>. URL <http://www.sciencedirect.com/science/article/pii/S0360128514000288>.
- [4] Yao M, Zheng Z and Liu H. Progress and recent trends in homogeneous charge compression ignition (hcci) engines. *Progress in Energy and Combustion Science* 2009; 35(5): 398 – 437. DOI:<http://dx.doi.org/10.1016/j.pecs.2009.05.001>. URL <http://www.sciencedirect.com/science/article/pii/S0360128509000197>.
- [5] Heywood JB. Fluid motion within the cylinder of internal combustion engines—the 1986 freeman scholar lecture. *Journal of Fluids Engineering* 1987; 109(1): 3–35. DOI:10.1115/1.3242612. URL <http://dx.doi.org/10.1115/1.3242612>.
- [6] Wickman D, Senecal P and Reitz RD. Diesel engine combustion chamber geometry optimization using genetic algorithms and multi-dimensional spray and combustion modeling. In *SAE 2001 Transactions Journal of Engines V110-3*. SAE International, 2001.
- [7] Wickman D, Yun H and Reitz RD. Split-spray piston geometry optimized for hsd diesel engine combustion. In *SAE 2003 Transactions Journal of Engines V112-3*. SAE International, 2003.
- [8] Miles PC and Andersson i. A review of design considerations for light-duty diesel combustion systems. *International Journal of Engine Research* 2015; DOI:10.1177/1468087415604754. URL <http://jer.sagepub.com/content/early/2015/10/04/1468087415604754.abstract>. <http://jer.sagepub.com/content/early/2015/10/04/1468087415604754.full.pdf+html>.
- [9] Dolak J, Shi Y and Reitz RD. A computational investigation of a stepped-bowl piston geometry for a light duty engine operating at low load. In *SAE 2010 World Congress and Exhibition*. 2010-01-1263, SAE International. DOI:10.4271/2010-01-1263.
- [10] Styron J, Baldwin B, Fulton B et al. Ford 2011 6.7l power stroke(r) diesel engine combustion system development. In *SAE 2011 World*

- Congress and Exhibition*. 2011-01-0415, SAE International, p. 7. DOI: 10.4271/2011-01-0415.
- [11] Kurtz EM and Styron J. An assessment of two piston bowl concepts in a medium-duty diesel engine. *SAE International Journal of Engines* 2012; 5(2): 344–352. DOI:10.4271/2012-01-0423. URL <http://saeeng.saejournals.org/content/5/2/344.abstract>. <http://saeeng.saejournals.org/content/5/2/344.full.pdf+html>.
- [12] Fridriksson H, Tuner M, Andersson O et al. Effect of piston bowl shape and swirl ratio on engine heat transfer in a light-duty diesel engine. In *SAE 2014 World Congress and Exhibition*. 2014-01-1141, SAE International, p. 13.
- [13] Dahlstrom J, Andersson O, Tuner M et al. Experimental comparison of heat losses in stepped-bowl and re-entrant combustion chamber in a light-duty diesel engine. In *SAE 2016 World Congress and Exhibition*. 2016-01-0732, SAE International, p. 12. DOI:10.4271/2016-01-0732.
- [14] Colban WF, Kim D, Miles PC et al. A Detailed Comparison of Emissions and Combustion Performance Between Optical and Metal Single-Cylinder Diesel Engines at Low Temperature Combustion Conditions. *SAE International Journal of Fuels and Lubricants* 2009; 1(1): 505–519. DOI:10.4271/2008-01-1066. URL <http://saefuel.saejournals.org/content/1/1/505.abstract>. <http://saefuel.saejournals.org/content/1/1/505.full.pdf+html>.
- [15] Ekoto IW, Colban WF, Miles PC et al. Uhc and co emissions sources from a light-duty diesel engine undergoing dilution-controlled low-temperature combustion. *SAE International Journal of Engines* 2010; 2(2): 411–430. DOI:10.4271/2009-24-0043. URL <http://saeeng.saejournals.org/content/2/2/411.abstract>. <http://saeeng.saejournals.org/content/2/2/411.full.pdf+html>.
- [16] Petersen BR, Ekoto IW and Miles PC. An investigation into the effects of fuel properties and engine load on uhc and co emissions from a light-duty optical diesel engine operating in a partially premixed combustion regime. *SAE International Journal of Engines* 2010; 3(2): 38–55. DOI: 10.4271/2010-01-1470. URL <http://saeeng.saejournals.org/content/3/2/38.abstract>. <http://saeeng.saejournals.org/content/3/2/38.full.pdf+html>.
- [17] Sahoo D, Petersen B and Miles P. Measurement of equivalence ratio in a light-duty low temperature combustion diesel engine by planar laser induced fluorescence of a fuel tracer. *SAE International Journal of Engines* 2011; 4(2): 2312–2325. DOI:10.4271/2011-24-0064. URL <http://saeeng.saejournals.org/content/4/2/2312.abstract>. <http://saeeng.saejournals.org/content/4/2/2312.full.pdf+html>.

- [18] Busch S, Zha K, Miles PC et al. Experimental and numerical investigations of close-coupled pilot injections to reduce combustion noise in a small-bore diesel engine. *SAE International Journal of Engines* 2015; 8(2): 660–678. DOI:10.4271/2015-01-0796. URL <http://saeeng.saejournals.org/content/8/2/660.abstract>. <http://saeeng.saejournals.org/content/8/2/660.full.pdf+html>.
- [19] Zha K, Busch S, Miles PC et al. Characterization of flow asymmetry during the compression stroke using swirl-plane piv in a light-duty optical diesel engine with the re-entrant piston bowl geometry. *SAE International Journal of Engines* 2015; 8(4): 1837–1855. DOI:10.4271/2015-01-1699. URL <http://saeeng.saejournals.org/content/8/4/1837.abstract>. <http://saeeng.saejournals.org/content/8/4/1837.full.pdf+html>.
- [20] Opat R. *Investigation of mixing and temperature effects on UHC/CO emissions for highly dilute low temperature combustion in a light-duty Diesel engine*. PhD Thesis, University of Wisconsin-Madison, 2006.
- [21] Perini F and Reitz RD. Introducing FRESCO: a fast, reliable engine simulation code. In *DOE AEC/HCCI Program Review Meeting, Southfield, MI, August 18-20 2015*.
- [22] Perini F, Miles PC and Reitz RD. A comprehensive modeling study of in-cylinder fluid flows in a high-swirl, light-duty optical diesel engine. *Computers & Fluids* 2014; 105: 113 – 124. DOI:<http://dx.doi.org/10.1016/j.compfluid.2014.09.011>. URL <http://www.sciencedirect.com/science/article/pii/S004579301400348X>.
- [23] Dempsey AB, Wang BL, Reitz RD et al. Comparison of Quantitative In-Cylinder Equivalence Ratio Measurements with CFD Predictions for a Light Duty Low Temperature Combustion Diesel Engine. *SAE International Journal of Engines* 2012; 5(2): 162–184. DOI:10.4271/2012-01-0143. URL <http://saeeng.saejournals.org/content/5/2/162.abstract>. <http://saeeng.saejournals.org/content/5/2/162.full.pdf+html>.
- [24] Perini F, Dempsey AB, Reitz RD et al. A Computational Investigation of the Effects of Swirl Ratio and Injection Pressure on Mixture Preparation and Wall Heat Transfer in a Light-Duty Diesel Engine. In *SAE 2013 World Congress and Exhibition*. DOI:10.4271:2013-01-1105. URL <http://papers.sae.org/2013-01-1105/>.
- [25] Han Z and Reitz RD. Turbulence Modeling of Internal Combustion Engines Using RNG k-epsilon Models. *Combustion Science and Technology* 1995; 106(4-6): 267–295. DOI:10.1080/00102209508907782. URL <http://dx.doi.org/10.1080/00102209508907782>. <http://dx.doi.org/10.1080/00102209508907782>.

- [26] Perini F and Reitz RD. Improved atomization, collision and sub-grid scale momentum coupling models for transient vaporizing engine sprays. *International Journal of Multiphase Flow* 2016; 79: 107 – 123. DOI: <http://dx.doi.org/10.1016/j.ijmultiphaseflow.2015.10.009>. URL <http://www.sciencedirect.com/science/article/pii/S0301932215002487>.
- [27] Perini F, Galligani E and Reitz RD. A study of direct and krylov iterative sparse solver techniques to approach linear scaling of the integration of chemical kinetics with detailed combustion mechanisms. *Combustion and Flame* 2014; 161(5): 1180 – 1195. DOI:<http://dx.doi.org/10.1016/j.combustflame.2013.11.017>. URL <http://www.sciencedirect.com/science/article/pii/S0010218013004306>.
- [28] Perini F, Galligani E and Reitz RD. An analytical jacobian approach to sparse reaction kinetics for computationally efficient combustion modeling with large reaction mechanisms. *Energy & Fuels* 2012; 26(8): 4804–4822. DOI:10.1021/ef300747n. URL <http://dx.doi.org/10.1021/ef300747n>.
- [29] Perini F, Zha K, Busch S et al. Principal Component Analysis and Study of Port-Induced Swirl Structures in a Light-Duty Optical Diesel Engine. In *SAE 2015 World Congress and Exhibition*. 2015-01-1696, SAE International, p. 19. DOI:10.4271/2015-01-1696. URL <http://papers.sae.org/2015-01-1696/>.
- [30] Zha K, Perini F, Busch S et al. Piston geometry effects on in-cylinder swirl asymmetry in a light-duty optical diesel engine. Technical Report SAND2015-7136C, Sandia National Laboratories (SNL-CA), Livermore, CA (United States), 2015. URL <http://www.osti.gov/scitech/servlets/purl/1311525>.
- [31] Zha K, Busch S, Park C et al. A novel method for correction of temporally- and spatially-variant optical distortion in planar particle image velocimetry. *Measurement Science and Technology* 2016; 27(8): 085201. URL <http://stacks.iop.org/0957-0233/27/i=8/a=085201>.
- [32] Perini F, Zha K, Busch S et al. Comparison of linear, non-linear and generalized rng-based k-epsilon models for turbulent diesel engine flows. In *SAE Technical Paper 2017-01-0561*. SAE International. DOI:10.4271/2017-01-0561. URL <http://doi.org/10.4271/2017-01-0561>.
- [33] Heywood J. *Internal Combustion Engine Fundamentals*. Automotive technology series, McGraw-Hill, 1988. ISBN 9780071004992.